

Twist-2 operators induced Dark Matter Interactions

Hrishabh Bharadwaj^{a,1,2}, Sukanta Dutta^{b,2}

¹*Department of Physics & Astrophysics, University of Delhi, New Delhi, India.*

²*SGTB Khalsa College, University of Delhi, New Delhi, India.*

Abstract We study the effective interactions of the fermionic, scalar and vector dark matter (DM) with leptons and neutral electroweak gauge Bosons induced by the higher dimensional effective twist-2 tensor operators. We constrain these lepto-philic, τ^\pm -philic and $U(1)_Y$ gauge Boson B-philic effective interactions of DM with the visible world from the WMAP and Planck data. The thermally averaged indirect DM pair annihilation cross-section and the spin-independent DM - free and/ or bound electron scattering cross-section are observed to be consistent with the respective experimental data. Constraining coefficients of the effective operators from the low energy LEP data for the $DM \leq 80$ GeV, we further study their sensitivities in the pair production of such $DM \geq 50$ GeV in association with di-jets and mono-photon respectively at the proposed ILC. We perform the χ^2 analysis to obtain the 99.73% C.L. acceptance contours in the $m_{DM} - A_{\text{eff}}$ plane from the two dimensional differential distributions of the kinematic observables and find that ILC has rich potential to probe the contribution of such effective operators.

Keywords Effective operators, lepto-philic, dark matter, linear collider, mono-photon.

PACS 95.35.+d, 13.66.-a, 13.66.De

1 Introduction

It is imperative to determine the nature of elusive *Dark Matter* (DM) [1] candidates, which constitute roughly $\sim 23\%$ of the energy density of the universe [1–6] and whose predicted relic density is ~ 0.119 [7, 8]. The most

popular proposition for DM theories are weakly interacting dark matter particles (WIMPs). Features of DM interactions can be determined from the direct and indirect detection experiments apart from their direct searches in the present [9–11] and proposed colliders [12–14]. The direct detection experiments like DAMA/LIBRA [15, 16], CoGeNT [17], CRESST [18], CDMS [19], XENON100 [20, 21], LUX [22] and PandaX-II [23] are designed to measure the recoil momentum of scattered atom or nucleon by DM in the chemically inert medium of the detector, while the indirect detection experiments such as FermiLAT [24–26], HESS [27], AMS-02 [28, 29] *etc.* are looking for the evidences of the DM pair annihilation to Standard Model (SM) particles such as photons, e^+e^- , $\mu^+\mu^-$, $\tau^+\tau^-$, $b\bar{b}$ pairs and *etc.*

In last few years, many experiments like PAMELA [30, 31] have reported the excess in the positron flux (i.e., flux ratio of positron to sum of electron and positron) without any significant excess in \bar{p} channel (i.e., flux ratio of protons to anti-protons). The peaks in e^+e^- channel are also observed in ATIC [32] and PPB-BETS [33] balloon experiments at around 1 TeV and 500 GeV respectively. Recently, Dark Matter Particle Explorer (DAMPE) experiment [34] has also observed a sharp peak around ~ 1.4 TeV favoring the lepto-philic DM annihilation cross-section of the order of $10^{-26} \text{cm}^3/\text{s}$. The excess in e^+e^- can be either due to astrophysical events like high energy emission from the pulsars or resulting from DM pair annihilation in our galactic neighborhood preferably to e^+e^- channel. Since the aforementioned experiments have not observed any significant excess in anti-proton channel, the DM candidates, if any, appears to be lepton friendly *lepto-philic* and have suppressed interaction with quarks at the tree level.

Various UV complete new physics extensions of SM have been proposed essentially to solve the gauge hier-

^aCorresponding Author,

e-mail: hrishabhphysics@gmail.com

^be-mail: Sukanta.Dutta@gmail.com

archy problem in the *top-down* approach which include theories like extra-dimensions [35], super-symmetry [36–38], little-Higgs [39, 40], extended 2-HDM models with singlets as portal of DM interactions [41] and *etc.* These models naturally provide the DM candidates or WIMPs, whose mass-scales are close to that of the electro-weak physics. However, the Direct detection experiments have shrunk the parameter space of the simplified and popular models where the WIMPs are made to interact with the visible world *via* neutral scalars and/ or gauge Bosons.

The model independent DM-SM particles interactions have also been studied in the *bottom-up* Effective Lagrangian approach where the mediator of DM-SM interactions are believed to be much heavier than the mass-scale of the lighter degrees of freedom say, in our case SM and DM particles [9–14]. The nature of these interactions are encapsulated in a set of coefficients corresponding to limited number of Lorentz and gauge invariant higher dimensional effective operators constructed with the light degrees of freedom. The constrained parameters (coefficients) space from various experimental data then essentially maps and direct towards the viable UV complete theoretical models. The generic effective Lagrangian for scalar, pseudo-scalar, vector, axial-vector interactions of SM particles with the scalar, vector, spin 1/2 and spin 3/2 dark matter candidates have been studied in literature [42–48].

Sensitivity analysis for DM-quark effective interactions at LHC have been performed [10, 11, 49–53] in a model-independent way for the dominant (a) mono-jet + \cancel{E}_T , (b) mono-*b* jet + \cancel{E}_T and (c) mono-*t* jet + \cancel{E}_T processes. Similarly, analysis for DM-gauge Boson effective couplings at LHC have been done by the authors in reference [54–56]. The sensitivity analysis of the coefficients and detailed analysis of detection cuts flow strategy for lepto-philic operators have also been performed through $e^+e^- \rightarrow \gamma + \cancel{E}_T$ [57–59] and $e^+e^- \rightarrow Z^0 + E_T$ [14, 60] channels.

Gross and Wilczek [61] analyzed the second rank twist operators appearing in the operator-product expansion of two weak currents along with the renormalization group equations of their coefficients for asymptotically free gauge theories in the context of deep inelastic lepton-hadron scattering. Later authors of reference [62] analysed the effective DM-nucleon scattering induced by twist-2 quark operators in the context of super-symmetric models where the Majorana DM particle neutralino being LSP was assumed to be much lighter than that of the squark masses. This was followed by series of papers [63–69] where the authors have calculated the one loop effect of DM-nucleon scattering induced by the twist-2 quarks and gluonic operators for the fermion,

vector and scalar DM respectively. The hadronic matrix elements induced by twist-2 operators can however be identified with the second moment of parton distribution functions and thus can be constrained from the available *pdfs*. This in turn constrain the coefficients of such higher dimensional effective operators to estimate the DM-nucleon scattering cross-sections for a suggested DM and squark mass range.

In this paper, we undertake the analysis for spin 1/2, 0 and 1 DM interactions induced by *lepto-philic* and $U(1)_Y$ gauge Boson *B-philic* effective twist-2 higher dimensional gauge invariant operators. This article is organized as follows: we formulate the effective interaction Lagrangian for fermionic, scalar and vector DM with SM leptons and neutral electro-weak gauge Bosons *via* twist-2 operators in section 2. In section 3, we constrain the coefficients of the effective Lagrangian from predicted relic density and perform a consistency check *w.r.t.* indirect and direct detection experiments. The constraints from the LEP on the coefficients of the effective lepto-philic and $U(1)_Y$ gauge Boson B-philic operators and the sensitivity analysis of these coefficients at the proposed ILC are discussed in section 4. Finally we summarize in section 5.

2 Effective interactions of lepto-philic & $U(1)_Y$ gauge Boson B-philic DM

We initiate the construction of the effective operators by writing the contact interaction between any SM leptons ψ and fermionic DM χ (Dirac or Majorana) with masses m_ψ and m_χ respectively, assuming that the mediator mass scale, if any, should be of the order of the cut-off of the effective theory ($\sim \Lambda$), which in general is much heavier than the masses of the SM and DM fields. These contact interactions for example can be motivated from the super-symmetric models where spin-independent neutralino-lepton interactions are facilitated by the exchange of heavy sleptons and/ or Higgses, assuming Majorana neutralino to be the LSP. For an illustration of such contact interactions, we write twist-2 Type-1 and Type-2 Lagrangians with the coupling strengths α_1 and α_2 respectively as:

$$\mathcal{L}_1 = \frac{1}{m_\chi} \frac{\alpha_1}{\Lambda^3} (\bar{\chi} \gamma^\mu \partial^\nu \chi) (\bar{\psi} \gamma_\mu \partial_\nu \psi - \partial_\nu \bar{\psi} \gamma_\mu \psi) \quad \text{and} \quad (1)$$

$$\mathcal{L}_2 = \frac{1}{m_\chi^2} \frac{\alpha_2}{\Lambda^3} (\bar{\chi} \partial^\mu \partial^\nu \chi) (\bar{\psi} \gamma_\mu \partial_\nu \psi - \partial_\nu \bar{\psi} \gamma_\mu \psi) \quad (2)$$

Using the equations of motion for massive Dirac fermions along-with the Tensor identity

$$P_{\mu\nu} Q^{\mu\nu} = (P_{\mu\nu} - \frac{1}{4} g_{\mu\nu} P^\alpha_\alpha) Q^{\mu\nu} + \frac{1}{4} P^\alpha_\alpha Q^\beta_\beta \quad (3)$$

the Lagrangians given in equations (1) and (2) can be re-written as

$$\mathcal{L}'_1 = \frac{1}{m_\chi} \frac{\alpha_1}{\Lambda^3} \left(-2i \mathcal{O}_{\mu\nu}^{(2)} \bar{\chi} \gamma^\mu \partial^\nu \chi - \frac{1}{2} m_\psi m_\chi \bar{\psi} \psi \bar{\chi} \chi \right) \quad (4)$$

$$\mathcal{L}'_2 = \frac{1}{m_\chi^2} \frac{\alpha_2}{\Lambda^3} \left(-2i \mathcal{O}_{\mu\nu}^{(2)} \bar{\chi} \partial^\mu \partial^\nu \chi - \frac{1}{2} m_\psi m_\chi \bar{\psi} \psi \bar{\chi} \chi \right) \quad (5)$$

respectively where $\mathcal{O}_{\mu\nu}^{(2)}$ is defined as trace-less twist-2 operator

$$\mathcal{O}_{\mu\nu}^{(2)} = \frac{i}{2} \left(\bar{\psi} \gamma_\mu \partial_\nu \psi + \bar{\psi} \gamma_\nu \partial_\mu \psi - \frac{g_{\mu\nu}}{2} \bar{\psi} \gamma^\alpha \partial_\alpha \psi \right) \quad (6)$$

and $\bar{\psi} \psi \bar{\chi} \chi$ appearing in the Eq.(6) is the scalar operator. The constraints on the four fermionic scalar DM operators has been extensively studied in the literature [14, 42]. However, the contributions of the tensor operators in equations (4) and (5) respectively are higher than those of the scalar operators due to the momentum dependence and therefore the coupling constants α_1 and α_2 would be comparatively more severely constrained for a given choice Cut-Off. Therefore it is worthwhile to probe the effect of these tensor operators in the DM pair annihilation and DM-electron or DM-Nucleon scatterings.

The twist-2 interactions of fermionic DM can also be realized through the twist-2 operators constructed out of SM charged and neutral electro-weak vector gauge Bosons $\mathcal{O}_{\mu\nu}^{V^{\text{EW}}} \equiv V^{\text{EW}\rho}{}_\mu V^{\text{EW}}{}_{\nu\rho} - \frac{1}{4} g_{\mu\nu} V^{\text{EW}}{}_{\rho\sigma} V^{\text{EW}\rho\sigma}$ and SM scalar Higgs Boson. Further the formalism can be extended to include the twist-2 Type-2 interactions of spin 0 and spin 1 DM particles with SM charged leptons and electro-weak gauge Bosons using equation (5). We analyse all such operators emerging from twist-2 interactions with SM charged leptons and neutral electro-weak gauge Bosons in this study.

There are other lepto-philic DM tensor operators which can have significant effect on DM phenomenology like dipole moments *etc.* as shown in references [70–72]. Since we are interested in operators which contribute to the spin independent non-relativistic DM - nucleon scattering process, we drop all the operators which are suppressed by the velocity of DM and/or nucleon. On using the equations of motions we expand all the interaction terms in the Lagrangian in powers of the super-weak coupling constant α_{T_i} . The spin-independent leading interactions in super-weak coupling expansion of the fermionic, vector and scalar DM operators are retained for analysis as explicitly shown in references [63–69] for the case of fermionic, vector and scalar DM operators interacting with quarks and gluons.

We enlist a minimal set of relevant twist-2 lepto-philic and $U(1)_Y$ gauge Boson B-philic operators in-

cluding contact interactions with Dirac fermion χ , real scalar ϕ^0 and real vector V_μ^0 DM candidates in the following Lagrangian:

$$\begin{aligned} \mathcal{L}_{\text{eff. Int.}}^{\text{DM}} &= \mathcal{L}_{\text{eff. Int.}}^{\text{spin } 1/2 \text{ DM}} + \mathcal{L}_{\text{eff. Int.}}^{\text{spin } 0 \text{ DM}} + \mathcal{L}_{\text{eff. Int.}}^{\text{spin } 1 \text{ DM}} \\ &= \sum_{p=l, B} \left[\sum_{T_i \in T_1, T_2} \frac{\alpha_{T_i}}{\Lambda^3} \mathcal{O}_{T_i}^p + \frac{\alpha_S}{\Lambda^2} \mathcal{O}_S^p + \frac{\alpha_V}{\Lambda^2} \mathcal{O}_V^p \right] \\ &= \sum_{p=l, B} \left[\sum_{T_i \in T_1, T_2} \frac{\lambda_{T_i}^\chi}{\Lambda_{\text{eff}}^3} \mathcal{O}_{T_i}^p + \frac{\lambda_{T_2}^{\phi^0}}{\Lambda_{\text{eff}}^2} \mathcal{O}_S^p + \frac{\lambda_{T_2}^{V^0}}{\Lambda_{\text{eff}}^2} \mathcal{O}_V^p \right] \end{aligned} \quad (7a)$$

where,

$$\mathcal{O}_{T_1}^p = \frac{1}{m_\chi} \bar{\chi} i \partial^\mu \gamma^\nu \chi \mathcal{O}_{\mu\nu}^p \quad (7b)$$

$$\mathcal{O}_{T_2}^p = \frac{1}{m_\chi^2} \bar{\chi} i \partial^\mu i \partial^\nu \chi \mathcal{O}_{\mu\nu}^p \quad (7c)$$

$$\mathcal{O}_S^p = \frac{1}{m_{\phi^0}^2} \phi^0 i \partial^\mu i \partial^\nu \phi^0 \mathcal{O}_{\mu\nu}^p \quad (7d)$$

$$\mathcal{O}_V^p = \frac{1}{m_{V^0}^2} V^{0\rho} i \partial^\mu i \partial^\nu V^0{}_\rho \mathcal{O}_{\mu\nu}^p \quad (7e)$$

The twist-2 operators $\mathcal{O}_{\mu\nu}^{l^\pm}$ for charged leptons $l^\pm \equiv e^\pm, \mu^\pm, \tau^\pm$ and $\mathcal{O}_{\mu\nu}^B$ for $U(1)_Y$ gauge field B^μ are defined in terms of the covariant derivative $D_\mu \equiv \partial_\mu + ig' B_\mu$ as

$$\mathcal{O}_{\mu\nu}^{l^\pm} \equiv i \frac{1}{2} \bar{l} \left(D_\mu \gamma_\nu + D_\nu \gamma_\mu - \frac{1}{2} g_{\mu\nu} \not{D} \right) l, \quad (8)$$

$$\mathcal{O}_{\mu\nu}^B \equiv B_\mu^\rho B_{\nu\rho} - \frac{1}{4} g_{\mu\nu} B_{\rho\sigma} B^{\rho\sigma}, \quad (9)$$

The cut-off scale of the effective theory Λ_{eff} is defined as $(4\pi)^{1/3} \Lambda$ and $\sqrt{4\pi} \Lambda$ for fermionic and Bosonic DM respectively. α_{T_i} and λ_{T_i} are the strengths and couplings of the interactions respectively, where $|\lambda_{T_i}| \leq \sqrt{4\pi}$ and $\Lambda \gtrsim 1$ TeV.

The Lorentz structure of the DM operators characterize the nature of DM pair annihilation and hence its contribution to the relic density [73]. Annihilation due to all operators given in equations (7) except fermionic Type 2 (7c) are found to be contributing to both s -wave and p -wave partial amplitudes, while Type 2 induced DM operator contributes to only p -wave amplitudes and hence comparatively suppressed. It is to be noted that the partial wave analysis of the annihilation processes induced by fermionic DM operators given in (7b) and (7c) remain same for both the Majorana type and/ or Dirac type because of the contact effective interactions.

We are now equipped to analyse and constrain these effective interactions from the DM phenomenology.

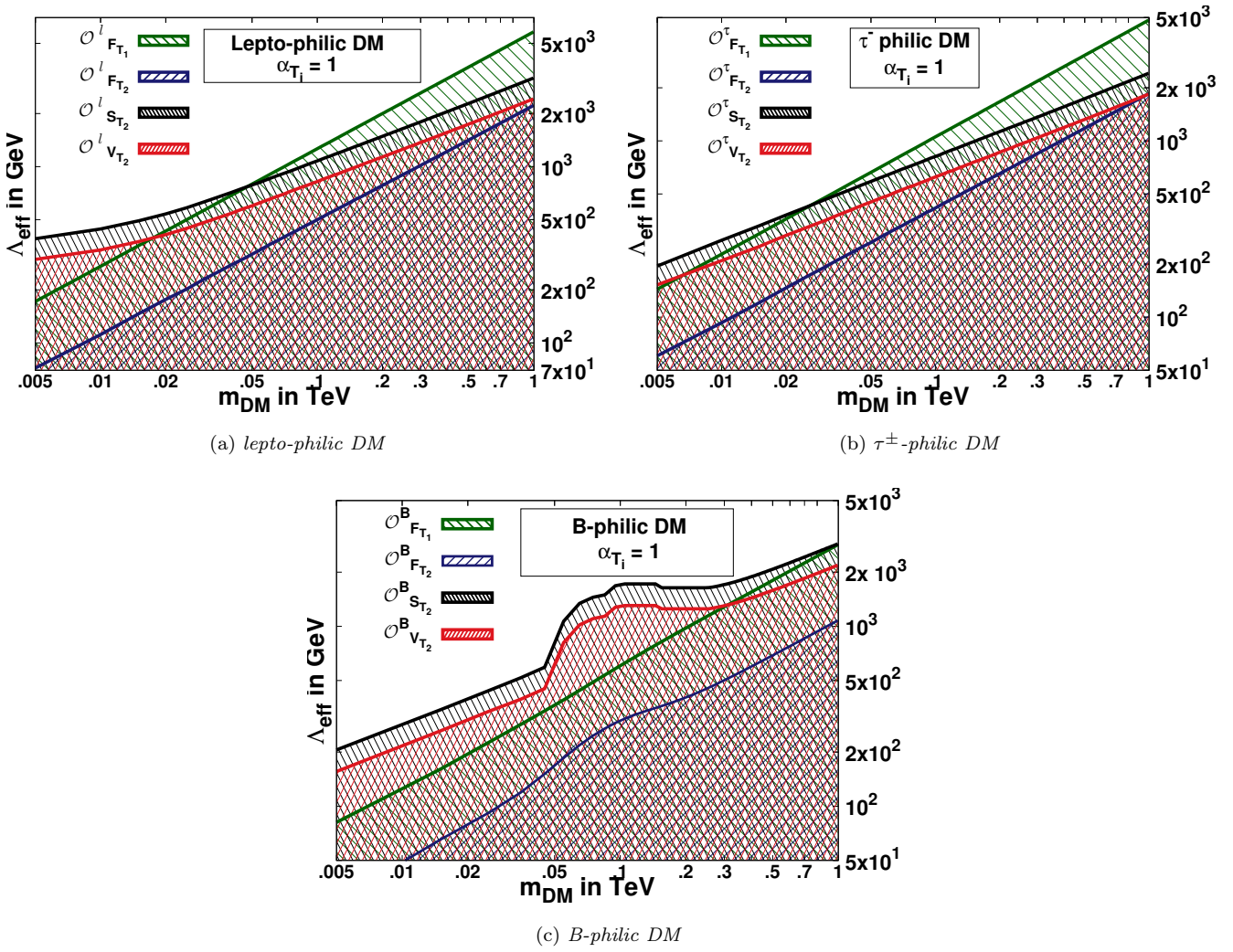


Fig. 1: Relic density contours are drawn using *MadDM v.3.0* [74] satisfying $\Omega_{\text{DM}} h^2 = 0.1199 \pm 0.0022$ [8] in the plane defined by DM mass and the respective upper bound on cut-off corresponding to the Type-1 or 2 twist operators at fixed coupling $\alpha_{T_i} = 1$. The respective shaded regions depict the allowed parameter space. Contours in figure 1a are depicted assuming the universal lepton flavor couplings of effective DM - SM lepton interactions.

3 DM Phenomenology

3.1 Constraints from Relic Density

In this sub-section we discuss the relic abundance of *lepto-philic* and *$U(1)_Y$ gauge Boson-philic* DM and constrain the effective interactions from the predicted DM relic density $\Omega_{\text{DM}} h^2$ of $0.1138 \pm .0045$ and 0.1199 ± 0.0022 by WMAP [7] and Planck [8] collaborations respectively. The current relic density for dark matter is calculated from the DM number density $n_{\text{DM}}(t)$ by solving the Boltzmann equation

$$\frac{d}{dt} n_{\text{DM}}(t) + 3\mathbf{H}(t) n_{\text{DM}}(t) = -\langle \sigma_{\text{ann}} |\mathbf{v}| \rangle [n_{\text{DM}}(t)^2 - n_{\text{DM}}^{\text{eq}}(t)^2] \quad (10)$$

where \mathbf{H} is the Hubble parameter, $\langle \sigma_{\text{ann}} |\mathbf{v}| \rangle$ is the thermal average of annihilation cross section multiplied by the relative velocity of dark matter pair. $n_{\text{DM}}^{\text{eq}}$ represents the dark matter number density in thermal equilibrium and is given by

$$n_{\text{DM}}^{\text{eq}} = \left[\mathbf{g} \left(\frac{m_{\text{DM}} T}{2\pi} \right)^{\frac{3}{2}} \exp \left\{ \frac{-m_{\text{DM}}}{T} \right\} \right]^{1/2} \quad (11)$$

where \mathbf{g} is the degrees of freedom. To numerically compute the current DM relic density we need to calculate the thermally averaged DM annihilation cross sections. Since the freeze-out for thermal relics occurs when the massive particle is non-relativistic *i.e.* $|\mathbf{v}| \ll c$, we make an expansion in $|\mathbf{v}|/c$ and then $\langle \sigma |\mathbf{v}| \rangle$ can be approximated as $\langle \sigma |\mathbf{v}| \rangle = a + b|\mathbf{v}|^2 + \mathcal{O}(|\mathbf{v}|^4)$.

Defining the dark matter relic abundance as a ratio of the thermal relic density ρ_{DM} and critical density of the universe $\rho_c = 1.05373 \times 10^{-5} \mathbf{h}^2 \text{ GeV}/(c^2 \text{cm}^3)$, where \mathbf{h} is the dimensionless Hubble parameter and solving the Boltzmann equation for the thermal relic density we get

$$\begin{aligned} \Omega_{\text{DM}} \mathbf{h}^2 &= \frac{\pi \sqrt{\mathbf{g}_{\text{eff}}(x_F)}}{\sqrt{90}} \frac{x_F T_0^3 \mathbf{g}_0}{M_{Pl} \rho_c \langle \sigma_{\text{ann}} v \rangle \mathbf{g}_{\text{eff}}(x_F)} \\ &\approx 0.12 \frac{x_F}{28} \frac{\sqrt{\mathbf{g}_{\text{eff}}(x_F)}}{10} \frac{2 \times 10^{-26} \text{cm}^3/\text{s}}{\langle \sigma |\mathbf{v}| \rangle} \end{aligned} \quad (12)$$

where M_{Pl} and \mathbf{g}_{eff} are Planck mass and effective number of degrees of freedom near the freeze-out temperature $T_F = \frac{m_{\text{DM}}}{x_F}$, where x_F is given by

$$x_F = \log \left[c' (c' + 2) \sqrt{\frac{45}{8}} \frac{\mathbf{g}_0 M_{Pl} m_{\text{DM}} \langle \sigma |\mathbf{v}| \rangle}{2 \pi^3 \sqrt{x_F} \mathbf{g}_{\text{eff}}(x_F)} \right] \quad (13)$$

where c' is a parameter of the order of one.

We have computed the thermal-averaged annihilation cross-section in the appendix for the Dirac fermion, a real scalar and real vector DM candidates. They are worked out in Appendix A. For τ^\pm -philic (electro-philic) case, all DM - leptons couplings except that of DM - τ^\pm (e^\pm) identically vanish.

To compute relic density numerically, we have used MadDM [74] and MadGraph [75]. We have generated the input model file required by MadGraph using FeynRules [76], which calculates all the required couplings and Feynman rules by using the full Lagrangian given in equation (7). We scan over the DM mass range 10 - 1000 GeV whose relic density satisfy $\Omega_{\text{DM}} \mathbf{h}^2 \leq 0.1199$ [8] for all vanishing interactions except one non-zero coupling α_{T_i} fixed at unity. We study and plot the relic density contours in the plane defined by DM mass and the cut-off corresponding to four (two fermionic, one scalar and one Vector DM) lepto-philic, τ^\pm -philic and B -philic operators in figures 1a, 1b and 1c respectively. We observe a bump around $m_{\text{DM}} \simeq 45\text{-}90$ GeV in figure 1c due to opening up of $Z \gamma$ and $Z Z$ annihilation channels induced by B philic DM operators. The increase in the total annihilation cross-section decreases the number density of the DM and as a result for a fixed DM relic density and coupling constant the contour shows a bump in the $m_{\text{DM}}\text{-}\Lambda$ plane. All points lying on the solid lines in figure ?? satisfy $\Omega_{\text{DM}} \mathbf{h}^2 \leq 0.1199$ [8]. These points are also the allowed upper limit on the cut-off for a given DM mass and thus the shaded region enclosed by the corresponding solid line is the cosmologically allowed parameter region of the respective operator. The lower value of the cut-off corresponding to the same DM mass will lead to only partial contribution to relic density and therefore may survive in model where (a) more than one type of DM particles are allowed and/ or (b) switching more than one type of effective operators

simultaneously. We observe that the sensitivity of the cut-off for fermionic Type-1 operator increases with the varying DM mass. Among the Type-2 operators, scalar DM cut-off is found to be the most sensitive. It is important to mention that the relic density contours for an electro-philic DM will be almost same to that of the τ^\pm -philic case.

3.2 Indirect Detection

Since the DM annihilation rate is proportional to the square of DM density, therefore DM annihilation is likely to be propelled in the over-dense region of the universe such as galactic center, dwarf spheroids and sun generate high flux of energetic light SM particles like charged hadrons, jets, the charged leptons *e.g.* electron, positron and photon. Since the non-relativistic DM particles are colliding at rest with each other, the energy of gamma-rays and the produced charged lepton is of the order of $\sim m_{\text{DM}}$. Indirect experiments which in general are either ground-based or satellite borne particle detectors are sensitive to these characteristic fluxes of light SM particles. For example FermiLAT (Large Area Telescope) is a space borne experiment designed to measure the tracks of electron-positron pairs which are produced when gamma-rays interact with the detector material (thin and high-Z foil) [24–26], while HESS is the ground based cherenkov telescope geared to detect the gamma ray spectrum [27].

In this section we calculate the thermally averaged annihilation cross sections for fermionic, real scalar and real vector Boson DM candidates to pair of charged leptons and photons. The analytical expressions for these cross-sections corresponding to the lepto-philic and $U(1)_Y$ gauge Boson B -philic operators are given in equations (A.10)-(A.13) and (A.14)-(A.17) respectively. We have used 220 Km/s (average rotational velocity of galaxy) as the average velocity of the DM.

The thermal averaged DM annihilation cross-section is computed numerically for a given set of parameter (m_{DM} , α_{T_i} , Λ_{eff}) which satisfy the relic density constraint from the Planck data as depicted in figure ??. For the lepto-philic and τ^\pm -philic operators we compute the dominant thermal averaged annihilation cross-section to $\tau^+ \tau^-$ pair using equations (A.10), (A.11), (A.12) and (A.13) corresponding to the fermionic DM Type-1 and Type-2, scalar DM Type-2 and vector DM Type-2 induced operators. The variation of the annihilation cross-section with the DM mass are depicted in figures 2a and 2b respectively. The solid lines in figures 2a and 2b are essentially the lower bound on the allowed annihilation cross-section satisfying the relic

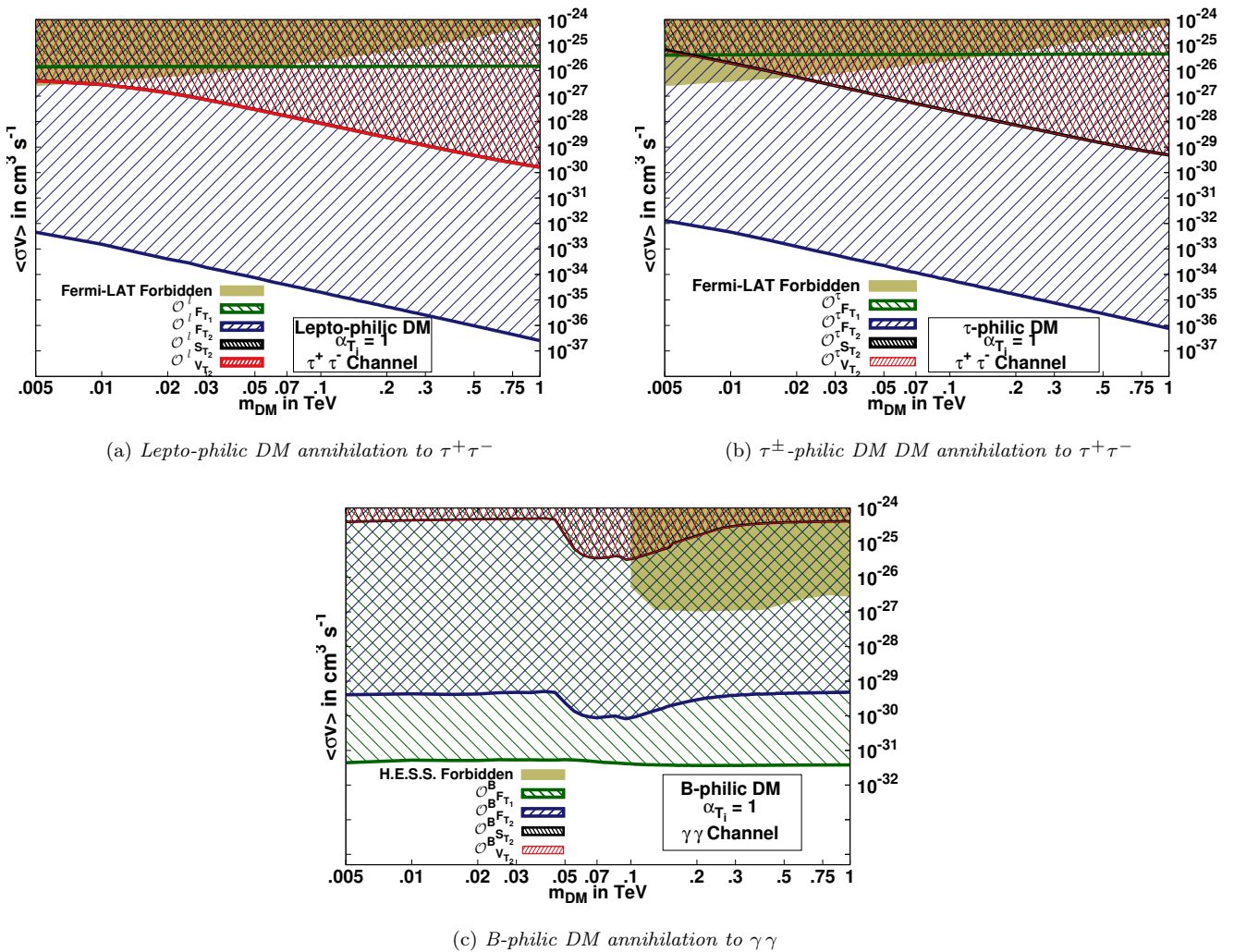


Fig. 2: Solid lines in all figures depict the variation of thermally averaged DM annihilation cross-sections w.r.t. the DM mass at the fixed coupling $\alpha_{T_i} = 1$ and the respective upper bound on the cut-off satisfying the relic density contribution. We plot the median of the DM annihilation cross section derived from a combined analysis of the nominal target sample for the $\tau^+\tau^-$ channel [26] in figures 2a, 2b and $\gamma\gamma$ [27] channel in figure 2c assuming a 100% branching fraction and thus restrict the respective allowed shaded region from above. Figure 2a shows the contours for the fermionic, scalar and vector DM interacting via Type-1 or 2 twist operators assuming the universal lepton flavor couplings with the DM.

density constraints for a given DM mass. It is interesting to note that although the analytical expression for the scalar and vector DM annihilation cross-section are not same but still we observe a complete overlap of the scalar and vector DM solid lines for $\alpha_{T_2}^{V^0} = \alpha_{T_2}^{\phi^0}$ which is an artifact of the two distinct values of the respective effective cut-off that satisfy the same relic density for a given DM mass. These results are compared with the upper bound on the allowed annihilation cross-section in $\tau^+\tau^-$ channel obtained from the FermiLAT data [26]. Thus the null experimental results for the given mass range translate into the lower limits on the cut-off for the respective operators.

The DM annihilation cross-section to the pair of electrons induced by the electro-philic DM are iden-

tical to those depicted in figure 2b for the respective operators.

For $U(1)_Y$ gauge Boson B-philic DM, we look for the photon pair production channel and the thermally averaged DM annihilation cross section is computed using equations (A.14), (A.15), (A.16) and (A.17) corresponding to the fermionic DM Type-1 and 2, scalar DM and vector DM Type-2 induced operators respectively. Figure 2c show the annihilation cross-sections depict in solid line for each case satisfying the relic density and thereby giving the lower bound on the cosmologically allowed annihilation cross-section. As in the case of lepto-philic and τ^\pm -philic, we observe that the scalar and vector annihilation cross-section overlaps for the reason mentioned earlier. We compare our results with

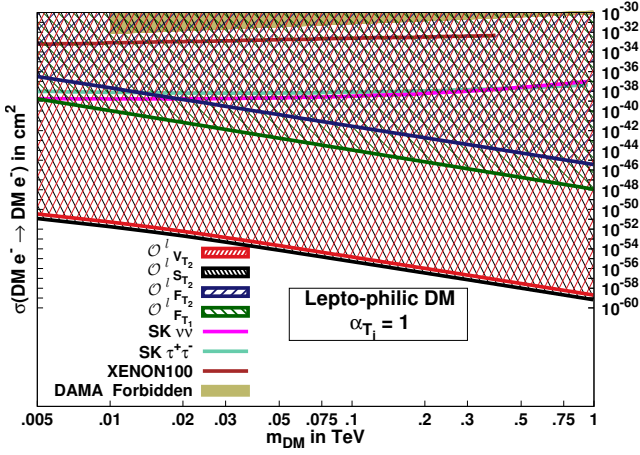


Fig. 3: Variation of DM - free electron elastic scattering cross-sections *w.r.t.* the DM mass at fixed lepton flavor universal coupling $\alpha_{T_i} = 1$ and the respective upper bound on the cut-off satisfying the relic density contribution for lepto-philic operators. The exclusion plots from DAMA at 90% C.L. for the case of DM-electron scattering are also shown [77]. Bounds at 90% C.L. are shown for XENON100 from inelastic DM-atom scattering [78]. The dashed curves show the 90% CL constraint from the Super-Kamiokande limit on neutrinos from the Sun, by assuming annihilation into $\tau^+\tau^-$ or $\nu\bar{\nu}$ [77].

that obtained from the null observation at HESS [27] for DM mass 100 GeV and above, which gives the upper lower bounds on the respective B-philic operators.

3.3 DM-electron scattering

Direct detection experiments [15–23] look for the scattering of nucleon or atom by DM particles. These experiments are designed to measure the recoil momentum of the nucleons or atoms of the detector material. These scattering can be broadly classified as (a) DM-electron scattering, (b) DM-atom scattering, and (c) DM-nucleus scattering. Since the lepto-philic, τ^\pm -philic and B-philic DM do not have direct interactions with quarks or gluons at tree level, therefore we explore tree level DM-electron elastic scattering induced by the lepto-philic operators only.

In this article, we restrict our study for those direct-detection processes which are realised at the tree level interactions of the lepto-philic DM operators with the free and bound electrons.

Consider the elastic (inelastic) scattering of non-relativistic DM having four-momentum k with free (bound) scattering cross-section with varying DM mass depicted in solid lines for Fermionic Type-1 and 2, scalar Type-2 & vector Type-2 twist-2 lepto-philic operators. The cross-section is computed for the coupling fixed at the unity and the corresponding cut-off which satisfy the relic density $\Omega_{\text{DM}}h^2 = 0.119$ [8] for a given DM mass.

erated matrix elements squared corresponding to the scattering processes induced by fermionic, scalar and vector lepto-philic operators:

$$\begin{aligned} |\overline{\mathcal{M}}_{free}^{\chi, T1}|^2 &= \frac{(4\pi\alpha_{T1}(k \cdot p))^2}{\Lambda_{\text{eff}}^6} 2 \left[m_{\text{DM}}^2 - k \cdot k' \right] \\ &\times \mathcal{F}_1 + \frac{p^2 k \cdot k' (m_e^2 + p \cdot p')}{4(k \cdot p)^2} + \frac{k' \cdot p (m_e^2 - 2p \cdot p')}{k \cdot p} \\ &- \frac{p^2 k' \cdot p'}{2(k \cdot p)} - \frac{p^2 (k \cdot p') (k' \cdot p)}{(k \cdot p)^2} + \frac{m_e^2 (k \cdot k')}{m_{\text{DM}}^2} \\ &- \frac{k \cdot k'}{m_{\text{DM}}^2} (p^2 k \cdot p' + 2p \cdot p') + \frac{2(k \cdot p) (k' \cdot p')}{m_{\text{DM}}^2} \\ &+ \frac{6(k \cdot p') (k' \cdot p)}{m_{\text{DM}}^2} \end{aligned}$$

where

$$\mathcal{F}_1 = \left[\frac{2m_e^2}{m_{\text{DM}}^2} + \frac{p^2(k \cdot p')}{m_{\text{DM}}^2} (k \cdot p) - \frac{p \cdot p'}{m_{\text{DM}}^2} - \frac{3p^2(p \cdot p')}{8(k \cdot p)^2} + \frac{5m_e^2 p^2}{8(k \cdot p)^2} \right] \quad (14a)$$

$$|\overline{\mathcal{M}}_{free}^{\chi, T2}|^2 = \frac{(4\pi\alpha_{T2} m_{\text{DM}}(k \cdot p))^2 \mathcal{F}'}{2\Lambda_{\text{eff}}^6} 4 \left(\frac{k \cdot k'}{m_{\text{DM}}^2} + 1 \right) \quad (14b)$$

$$|\overline{\mathcal{M}}_{free}^{\phi^0, T2}|^2 = \frac{(4\pi\alpha_{T2}(k \cdot p))^2}{\Lambda_{\text{eff}}^4} \times \mathcal{F}' \quad (14c)$$

$$|\overline{\mathcal{M}}_{free}^{V^0, T2}|^2 = \frac{(4\pi\alpha_{T2}(k \cdot p))^2 \mathcal{F}'}{3\Lambda_{\text{eff}}^4} \left(\frac{(k \cdot k')^2}{m_{\text{DM}}^4} + 2 \right)$$

where

$$\mathcal{F}' = \left[\frac{m_e^2}{m_{\text{DM}}^2} - \frac{p^2}{m_{\text{DM}}^2} \frac{k \cdot p'}{k \cdot p} - 2 \frac{p \cdot p'}{m_{\text{DM}}^2} + 4 \frac{k \cdot p}{m_{\text{DM}}^2} \frac{k \cdot p'}{m_{\text{DM}}^2} + \frac{1}{8} \frac{p^2 (p \cdot p' + m_e^2)}{(k \cdot p)^2} \right] \quad (14d)$$

The corresponding scattering cross-sections of DM with the free electron at rest are given as

$$\sigma_{T1}^{\chi e} = 36\pi\alpha_{T1}^2 \frac{m_e^4}{\Lambda_{\text{eff}}^6} \quad (15a)$$

$$\sigma_{T2}^{\chi e} = 36\pi\alpha_{T2}^2 \frac{m_e^4}{\Lambda_{\text{eff}}^6} \quad (15b)$$

$$\sigma_{T2}^{\phi^0 e} = 9\pi \frac{\alpha_{\phi^0}^2}{\Lambda_{\text{eff}}^4} \frac{m_e^4}{m_{\phi^0}^2} \quad (15c)$$

$$\sigma_{T2}^{V^0 e} = 9\pi \frac{\alpha_{V^0}^2}{\Lambda_{\text{eff}}^4} \frac{m_e^4}{m_{V^0}^2} \quad (15d)$$

In figure 3 we plot the DM - free electron elastic scattering cross-section with varying DM mass depicted in solid lines for Fermionic Type-1 and 2, scalar Type-2 & vector Type-2 twist-2 lepto-philic operators. The cross-section is computed for the coupling fixed at the unity and the corresponding cut-off which satisfy the relic density $\Omega_{\text{DM}}h^2 = 0.119$ [8] for a given DM mass.

Although the analytical expressions of the scattering cross-sections corresponding to the Type I and Type II twist interactions of the fermionic DM are similar but we observe the two distinct solid lines corresponding to these contributions in figure 3 because of the different values of the respective cut-offs contributing to the same relic density for a given DM mass when $\alpha_{T_1} = \alpha_{T_2}$. Same reason holds for the observed distinguishable contributions from scalar and vector DM scattering cross-sections respectively in figure 3 for $\alpha_{T_2}^{V^0} = \alpha_{T_2}^{\phi^0}$ although the corresponding analytical expressions are same. These results are then compared with the null results of DAMA/LIBRA [15, 16] at 90% confidence level for DM-electron scattering and XENON100 [20, 21] at 90% confidence level for inelastic DM-atom scattering.

It is important to note that electro-philic DM -free electron scattering cross-sections corresponding to the respective operators computed using the upper bound on the cut-off obtained for a given DM mass from relic density constraints as shown in figure 1b and unity coupling strength, will be slightly higher than those shown in the figure 3.

The DM - free electron scattering corresponding to the τ^\pm -philic and B -philic operators occurs at the one loop level and therefore are further suppressed. On the same note, due to the absence of the tree level DM - quark interactions, DM-nucleon scattering induced by the lepto-philic and $U(1)_Y$ -philic twist-2 operators are either one or two loop(s) suppressed, however it dominates over the DM-free (bound) electron scattering.

3.3.1 Inelastic scattering : Effect of bound electrons

The non-relativistic DM ($E_{DM} \sim m_{DM}$) essentially collides the bound electron of fixed energy $E_e = m_e - E_B^{nl}$ (here E_B^{nl} is the binding energy of electron in l^{th} orbital of n^{th} shell) and momentum distribution \mathbf{p} and then finally ejects the electron from the atom with the energy $E_R + m_e - E_B^{nl}$, where E_R is the recoil energy of the scattered electron. The inelastic DM - electron differential scattering cross-section *w.r.t.* the recoil energy in the lab frame is computed to be

$$\begin{aligned} \frac{d\sigma_{nlm}}{dE_R} &= \frac{|\overline{\mathcal{M}}_{nlm}|^2}{32\pi E_{DM} E_e v_{rel} |\mathbf{k} + \mathbf{p}|} \\ &= \frac{|\chi_{nl}(|\mathbf{p}|)|^2 |Y_{lm}(\theta, \phi)|^2 |\overline{\mathcal{M}}_{free}|^2}{32\pi E_{DM} E_e v_{rel} |\mathbf{k} + \mathbf{p}|} \end{aligned} \quad (16)$$

where $\chi_{nl}(|\mathbf{p}|)$ is the l^{th} radial momentum space wavefunction for n^{th} shell and $Y_{lm}(\theta, \phi)$ is the angular wavefunction associated with the bound electron. Summing over all possible shells (which depends on the detector

material),

$$\sum_{nlm} \frac{d\sigma_{nlm}}{dE_R} = \sum_{nl} \frac{|\chi_{nl}(|\mathbf{p}|)|^2 |\overline{\mathcal{M}}_{free}|^2 (2l+1)}{32\pi E_{DM} E_e v_{rel} |\mathbf{k} + \mathbf{p}| 4\pi} \quad (17)$$

Following the prescription given in the appendixes **B** and **C** of reference [77] we estimate the total event rate as

$$\frac{dR}{dE_R} = \frac{\rho_0 n_T}{m_{DM}} \int \frac{d^3p}{(2\pi)^3} \int d^3v v_{rel} f_\odot(\mathbf{v}) \sum_{nlm} \frac{d\sigma_{nlm}}{dE_R} \quad (18)$$

where ρ_0 , n_T , $f_\odot(\mathbf{v})$ and v_{rel} are local density of DM ($\approx 0.3 \text{ GeV}/\text{cm}^3$), number of target particles per unit mass, velocity distribution of DM in lab frame and relative velocity of DM and bound electron respectively. Substituting (17) and using **NaI** as the detector material [16], we compute the event rate as

$$\frac{dR}{dE_R} = \frac{\rho_0}{64\pi m_{DM}^3 m_e (m_I + m_{Na})} \sum_{n,l} \epsilon_{nl} \eta(v_{min}) |\overline{\mathcal{M}}_{free}|^2 \quad (19)$$

where $\eta(v_{min}) \equiv \int d^3v \frac{f_\odot(\mathbf{v})}{v} \theta(v - v_{min})$ with $v_{min} \approx \frac{E_R}{|\mathbf{p}|} + \frac{|\mathbf{p}|}{m_{DM}}$ and ϵ_{nl} is the suppression factor

$$\epsilon_{nl} = \sqrt{2m_e (E_R - E_B^{nl})} (2l+1) \int \frac{dp}{(2\pi)^3} |\mathbf{p}| |\chi_{nl}(|\mathbf{p}|)|^2 \quad (20)$$

For the detector signal with the deposited energy $\sim E_R = 2 - 4 \text{ keV}$, which is sensitive to the DAMA/LIBRA experiment, the integral in equation (20) is found to be maximum for the electron corresponding to the $3s$ orbital of Iodine $\sim 10^{-2} \text{ MeV}^{-1}$ for **NaI** crystals. Substituting the binding energy of $3s$ electron of Iodine $\sim 1 \text{ keV}$, the suppression factor becomes $\sim 10^{-6}$.

It is important to mention that the event rates from lepto and $U(1)_Y$ -philic induced DM-nucleon scattering which are suppressed by $\sim (\alpha_{em} Z/\pi)^2$, where Z is charge of the nucleus at one loop order, are however do not have any wave-function suppression.

4 Collider sensitivity of effective operators

4.1 LEP Constraints on the effective operators

We investigate the constraints on the lepto-philic and B -philic effective operators from the existing results and observations from LEP data. We compute the cross-section for the process $e^+e^- \rightarrow \gamma^* + \text{DM pair}$, and compare with the combined analysis from DELPHI and L3 collaborations for $e^+e^- \rightarrow \gamma^* + Z \rightarrow q_i \bar{q}_i + \nu_{l_j} \bar{\nu}_{l_j}$ at $\sqrt{s} = 196.9 \text{ GeV}$ and an integrated luminosity of 679.4 pb^{-1} , where $q_i \equiv u, d, s$ and $\nu_{l_j} \equiv \nu_e, \nu_\mu, \nu_\tau$. The mea-

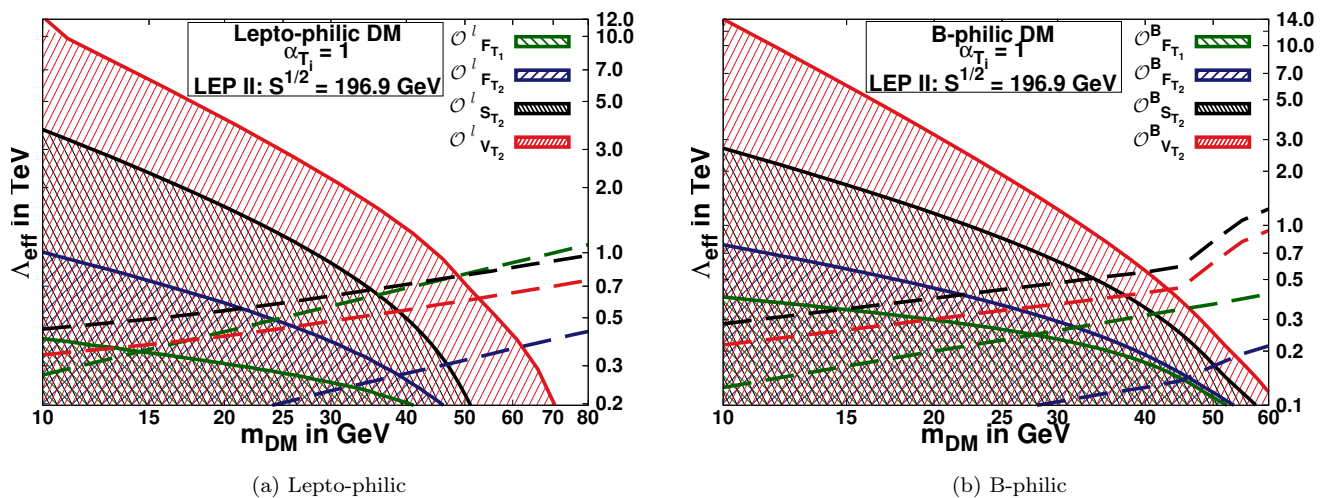


Fig. 4: Solid lines depict the contours in the plane defined by DM mass and the kinematic reach of the cut-off Λ_{eff} for $e^+e^- \rightarrow \text{DM pairs} + \gamma^* \rightarrow \cancel{E}_T + q_i \bar{q}_i$ at fixed coupling $\alpha_{T_i} = 1$, $\sqrt{s} = 196.9 \text{ GeV}$ and an integrated luminosity of 679.4 pb^{-1} , satisfying the constraint $\delta\sigma_{\text{tot}} = .032 \text{ pb}$ obtained from combined analysis of DELPHI and L3 [79]. The enclosed shaded region corresponding to each solid line are forbidden by LEP observation. The regions below the colored dashed lines corresponding to respective four operators satisfy the relic density constraint $\Omega_{\text{DM}} h^2 \leq 0.1199 \pm 0.0022$.

sured cross-section from the combined analysis for the said process is found to be $.055 \text{ pb}$ along with the measured statistical error $\delta\sigma_{\text{stat}}$, systematic error $\delta\sigma_{\text{sys}}$ and total error $\delta\sigma_{\text{tot}}$ of $.031 \text{ pb}$, $.008 \text{ pb}$ and $.032 \text{ pb}$ respectively [79]. Therefore, contribution due to an additional channel containing the final states DM pairs and resulting into the missing energy along with two quark jets can be constrained from the observed $\delta\sigma_{\text{tot}}$.

In figures 4a and 4b, we plot the 95% C.L. solid line contours satisfying the cross-section observed $\delta\sigma_{\text{tot}}$ $.032 \text{ pb}$ corresponding to the lepto-philic and B-philic operators in the two dimensional plane defined by the DM mass and the lower bound on the cut-off at the fixed value of respective coupling α_{T_i} . The respective shaded regions in figure 4 are disallowed by the combined LEP analysis. Thus the phenomenologically interesting DM mass range $\lesssim 50 \text{ GeV}$ is completely disfavored by the LEP experiments.

4.2 Constraints from LHC Observations

Some of the interesting signatures of DM are missing energy \cancel{E}_T on transverse plane with Jets, photons, Z^0 or any other visible SM particles. For lepto-philic and B-philic DM cases we consider $pp \rightarrow (Z^0 \rightarrow l^+ l^-) + \cancel{E}_T$ and $pp \rightarrow \cancel{E}_T \gamma$ processes at the LHC respectively [10, 49]. The recent analysis of $pp \rightarrow l^+ l^- l^+ l^-$ at $\sqrt{s} = 8 \text{ TeV}$ for both CMS [50] and ATLAS [51] showed that the measured events are consistent with SM and an integrated luminosity of 20.7 fb^{-1} . However, in ref-

erence [52] the authors have shown that the contribution of lepto-philic DM dimension six operators can be strongly constrained at $\sqrt{s} = 14 \text{ TeV}$ for the DM mass $\leq 250 \text{ GeV}$. We believe the enhancement in the centre of mass energy and luminosity will enable both the detectors to probe the sensitivity of the lepto-philic twist operators.

Recently the ATLAS Collaboration [80] has reported the events containing an energetic photon and large missing transverse momentum for BSM searches at $\sqrt{s} = 13 \text{ TeV}$ and an integrated luminosity of 36.1 fb^{-1} which agrees with SM predictions within the systematic and statistical uncertainty. The SM background contribution arises from $pp \rightarrow Z(\rightarrow \nu\bar{\nu}) \gamma$, $pp \rightarrow W(\rightarrow l\nu) \gamma$, $pp \rightarrow Z(\rightarrow l l) \gamma$ and $pp \rightarrow \gamma + \text{jets}$ processes. The events containing fake photons coming from electrons and jets are also included in the analysis. The experimental observations constrain the contribution of the effective operators and put an upper bound on disallowed Λ_{eff} for DM coupling fixed at unity and a given DM mass due to non-observation of any appreciable change in SM predicted Events.

4.3 \cancel{E}_T + Mono-photon signals at ILC

We consider following DM production processes along with on/ off shell photon at the proposed ILC, for the DM mass range $\sim 50 - 500 \text{ GeV}$: (a) $e^+e^- \rightarrow \chi \bar{\chi} \gamma / \gamma^*$, (b) $e^+e^- \rightarrow \phi^0 \phi^0 \gamma / \gamma^*$, and (c) $e^+e^- \rightarrow V^0 V^0 \gamma / \gamma^*$. The dominant SM background for $e^+e^- \rightarrow \cancel{E}_T + \gamma / \gamma^*$

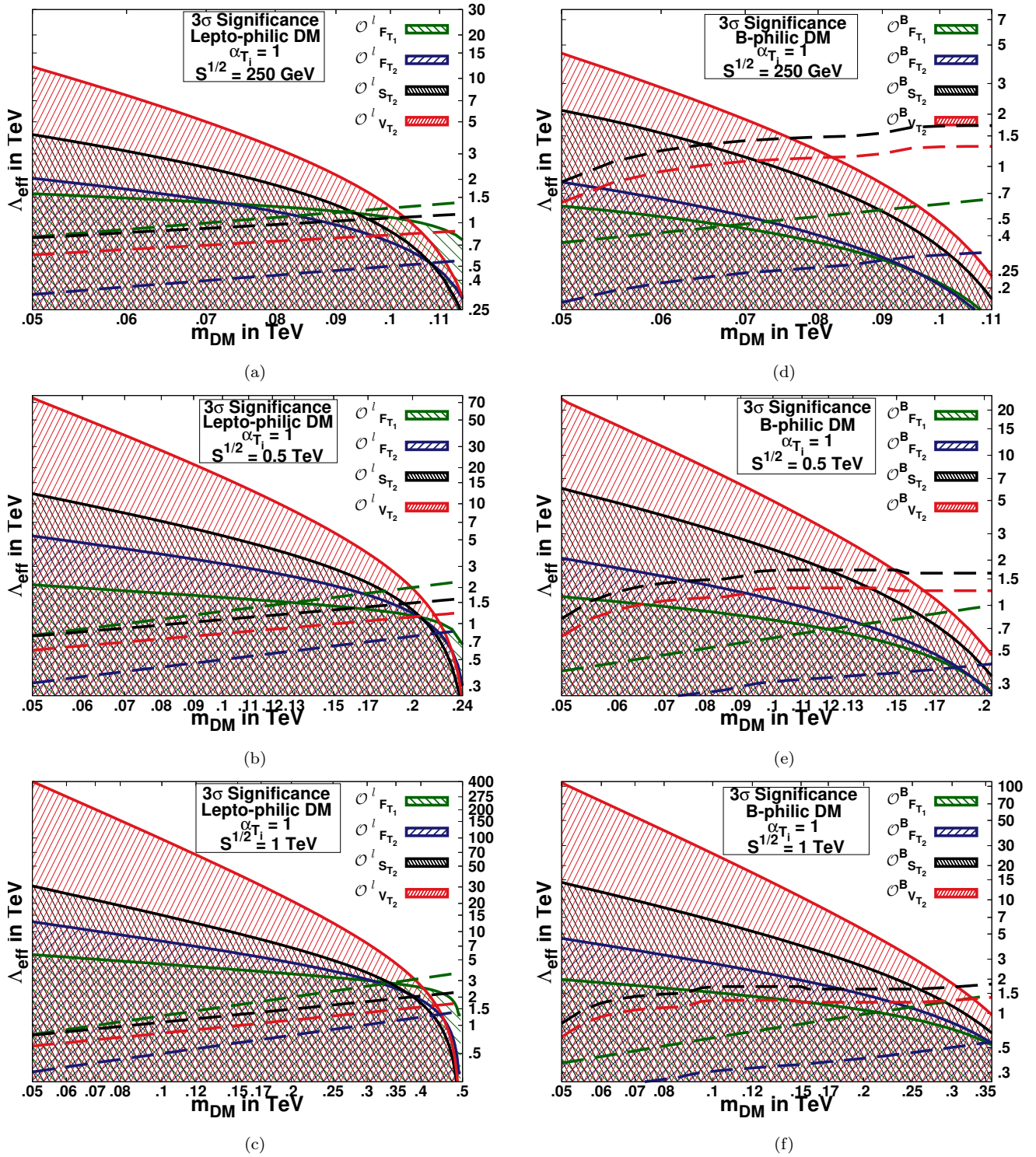


Fig. 5: Solid lines depict 3σ efficiency contours at fixed coupling $\alpha_{T_i} = 1$ for DM pair production process with mono-photon ($e^+e^- \rightarrow F_T + \gamma$) in the plane defined by DM mass and the kinematic reach of the cut-off Λ_{eff} corresponding to (a) $\sqrt{s} = 250$ GeV; $\mathcal{L} = 250 \text{ fb}^{-1}$ in 5a and 5d, (b) $\sqrt{s} = 500$ GeV; $\mathcal{L} = 500 \text{ fb}^{-1}$ in 5b and 5e and (c) $\sqrt{s} = 1$ TeV; $\mathcal{L} = 1 \text{ ab}^{-1}$ in 5c and 5f. The shaded region corresponding to each solid line are likely to be probed by ILC with greater than 3σ efficiency. The regions below the colored dashed lines corresponding to respective four operators satisfy the relic density constraint $\Omega_{\text{DM}} h^2 \leq 0.1199 \pm 0.0022$.

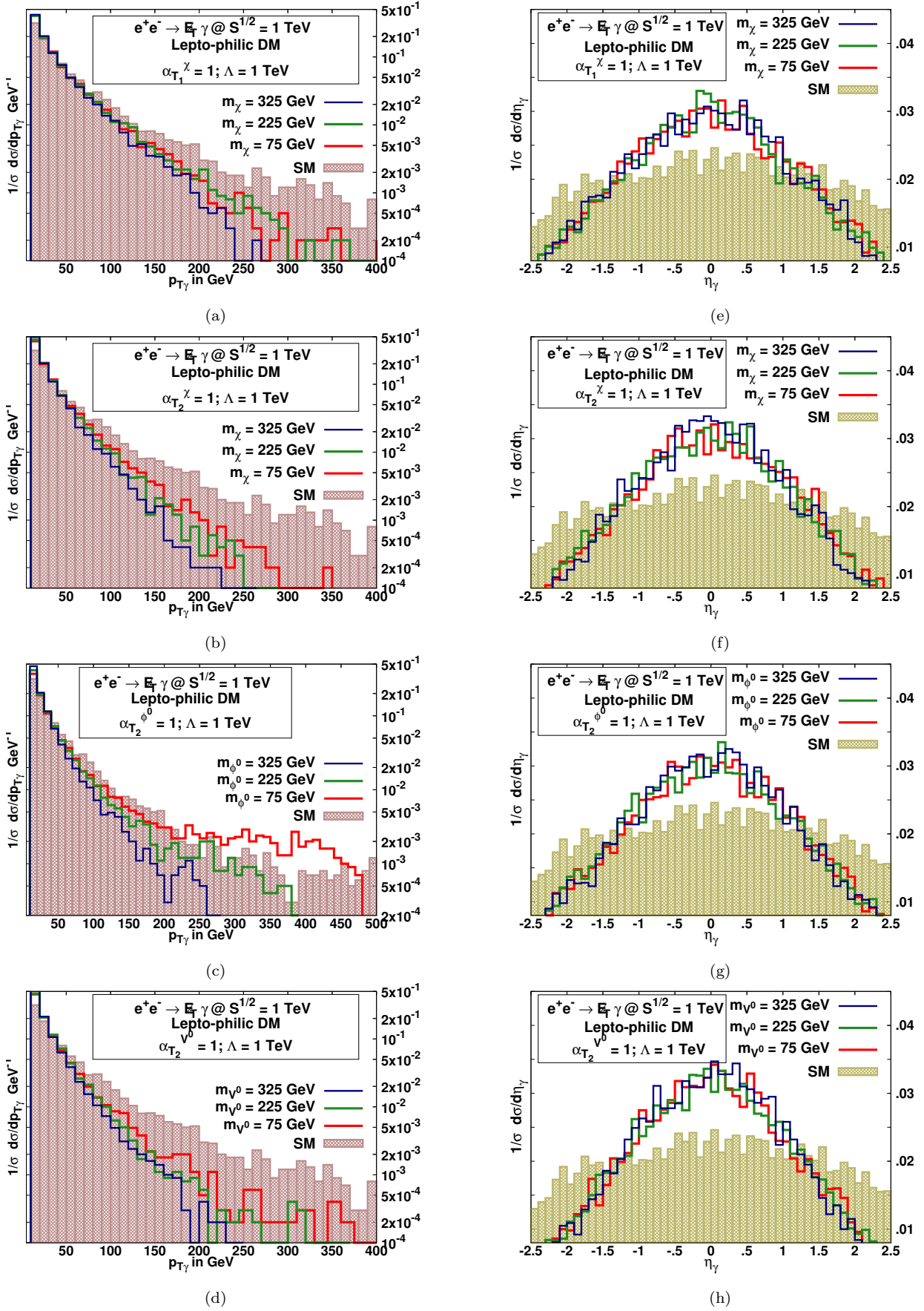


Fig. 6: Normalized 1-D differential cross-sections *w.r.t.* $p_{T\gamma}$ (bin width 10 GeV) and η_γ (bin width 0.1) corresponding to the SM processes (shaded histograms) and those induced by lepto=philic operators at the three representative values of DM masses: 75, 225 and 325 GeV respectively.

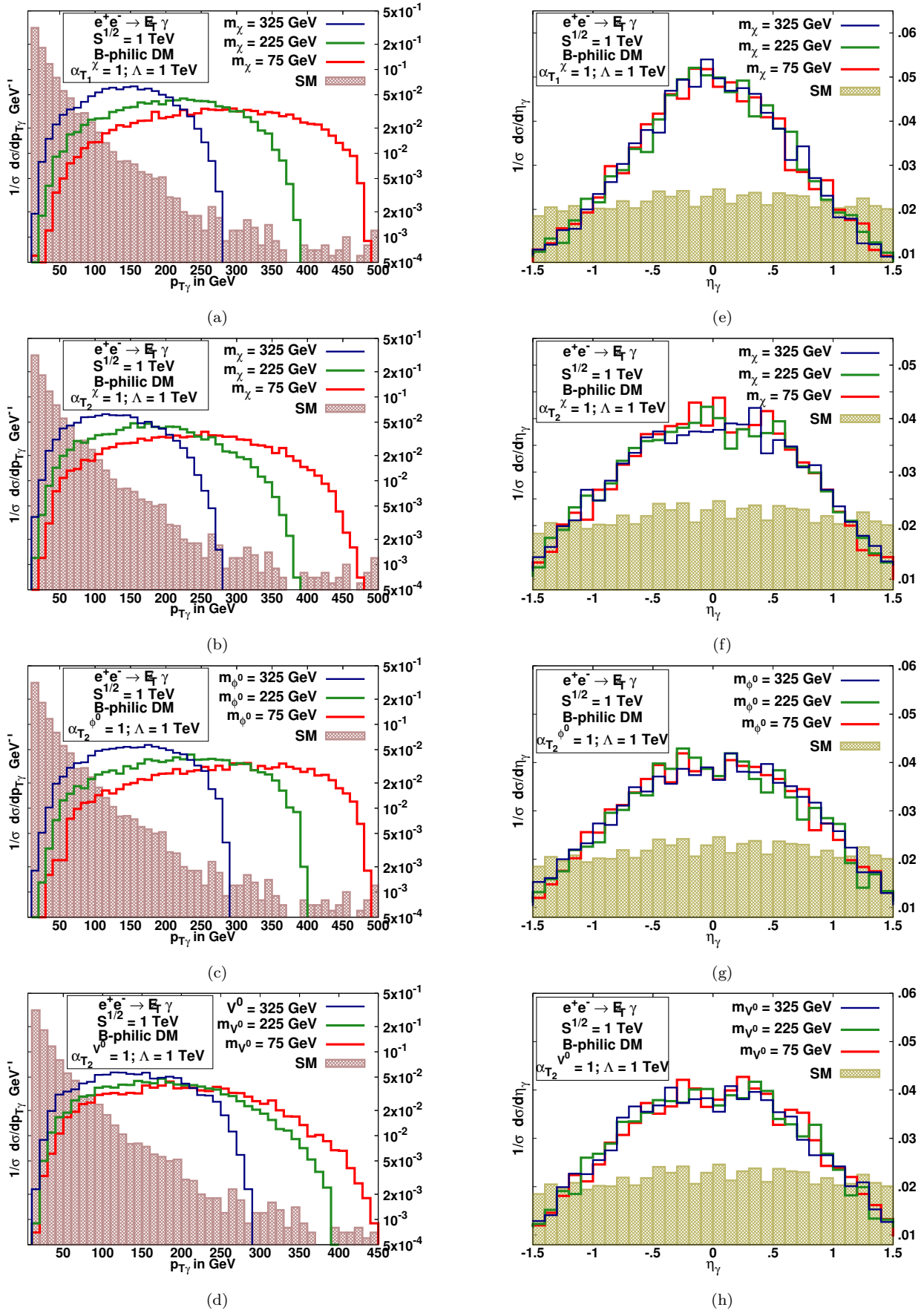


Fig. 7: Normalized 1-D differential cross-sections *w.r.t.* p_{T_γ} (bin width 10 GeV) and η_γ (bin width 0.1) corresponding to the SM processes (shaded histograms) and those induced by B-philic operators at the three representative values of DM masses: 75, 225 and 325 GeV respectively.

	<i>ILC-250</i>	<i>ILC-500</i>	<i>ILC-1000</i>
\sqrt{s} (in GeV)	250	500	1000
L_{int} (in fb ⁻¹)	250	500	1000
σ_{bg} (pb)	1.07	1.48	2.07

Table 1: Accelerator parameters as per *Technical Design Report* [81, 82]. σ_{bg} is the background cross section for $e^- e^+ \rightarrow \sum \nu_i \bar{\nu}_i \gamma$ process computed using the selection cuts defined in section 4.3

ILC Parameters: $\sqrt{s} = 1$ TeV; $L = 1000$ fb ⁻¹						
Process:	$e^+ e^- \rightarrow \cancel{E} \gamma^* (\gamma^* \rightarrow jj)$			$e^+ e^- \rightarrow \cancel{E} \gamma$		
Cuts:	$ m_{j_1 j_2} \leq \sqrt{m_Z^2 - 5\Gamma_Z m_Z}$ $\cancel{E}_T \geq \sqrt{m_Z^2 + 5\Gamma_Z m_Z}$			$\frac{2E_\gamma}{\sqrt{s}} \notin [0.98, 0.99]$		
Operators	75 GeV	225 GeV	325 GeV	75 GeV	225 GeV	325 GeV
$\mathcal{O}_{F_{T_1}}^L$	3.4	2.3	1.9	3.9	2.7	2.3
$\mathcal{O}_{F_{T_2}}^L$	8.2	3.5	2.3	9.7	4.2	2.8
$\mathcal{O}_{S_{T_2}}^L$	9.2	4.6	2.4	20.2	5.7	3.1
$\mathcal{O}_{V_{T_2}}^L$	135.5	12.2	4.3	175.4	16.1	5.8
$\mathcal{O}_{F_{T_1}}^B$	1.8	1.1	0.7	2.5	0.9	0.6
$\mathcal{O}_{F_{T_2}}^B$	3.7	1.4	0.8	3.4	1.2	0.7
$\mathcal{O}_{S_{T_2}}^B$	10.2	2.4	1.1	9.1	2.1	0.9
$\mathcal{O}_{V_{T_2}}^B$	9.5	4.7	1.6	46.6	4.0	1.4

Table 2: 3σ significance upper bound on Λ_{eff} in TeV with respective α_{T_i} fixed at unity for given three choices of $m_{\text{DM}} \equiv 75, 225$ and 325 GeV respectively.

signature comes from $Z^0 \gamma$ production process: $e^+ e^- \rightarrow Z^0 + \gamma / \gamma^* \rightarrow \sum \nu_i \bar{\nu}_i + \gamma / \gamma^*$.

The analysis for the background and the signal processes corresponding to the accelerator parameters as conceived in the *Technical Design Report for ILC* [81, 82] and given in Table 1 is performed by simulating SM backgrounds and the DM signatures using Madgraph [75] and the model file generated by FeynRules [76]. We impose the basic selection cuts $\cancel{E}_T \geq \sqrt{m_Z^2 + 5\Gamma_Z m_Z}$ and $|m_{j_1 j_2}| \leq \sqrt{m_Z^2 - 5\Gamma_Z m_Z}$ to reduce the backgrounds for the process $e^+ e^- \rightarrow \cancel{E} \gamma^* (\gamma^* \rightarrow jj)$. On the same note, we impose the following cuts to reduce the backgrounds for the DM pair production in association with mono-photon:

- Transverse momentum of photon $p_{T_\gamma} \geq 10$ GeV,
- Pseudo-rapidity of photon is restricted as $|\eta_\gamma| \leq 2.5$,
- dis-allowed recoil photon energy against on-shell Z^0 $\frac{2E_\gamma}{\sqrt{s}} \notin [0.8, 0.9], [0.95, 0.98]$ and $[0.98, 0.99]$ for $\sqrt{s} = 250$ GeV, 500 GeV and 1 TeV respectively.

As a first step towards preliminary analysis we study the significance \mathcal{S} for the DM production processes, defined as

$$\mathcal{S} = \frac{N_S}{\sqrt{N_B + (\delta_{\text{sys}} N_B)^2}} \quad (21)$$

where N_S is the number of DM with mono-photon events, N_B is the number of SM background events and δ_{sys}

is the systematic error. We compare the three sigma significance of the DM pair production with associated with On/ Off-shell photons, for three representative values of DM mass 75, 225, and 325 GeV respectively. We give the kinematic reach of Λ_{eff} corresponding to all cases of scalar, fermionic and vector DM based on the 3σ efficiency in table 2 and find that mono photon signatures gives the better kinematic reach of Λ_{eff} for a given coupling and mass of the DM. Therefore, we restrict our analysis for the DM pair production with associated with mono-photons.

The 3σ sensitivity contours in $\Lambda_{\text{eff}} - m_{\text{DM}}$ plane are drawn for the DM production cross-sections with $\alpha_{T_i} = 1$ and conservative $\delta_{\text{sys}} \sim 1\%$ in figures 5a, 5d, 5b, 5e, 5c and 5f. Figures 5a and 5d correspond to lepto-philic and B-philic operators respectively for the proposed ILC at $\sqrt{s} = 250$ GeV at an integrated luminosity of 250 fb^{-1} , figures 5b and 5e correspond to lepto-philic and B-philic operators respectively for the proposed ILC at $\sqrt{s} = 500$ GeV at an integrated luminosity of 500 fb^{-1} , and figures 5c and 5f respectively depict the same for $\sqrt{s} = 1$ TeV at an integrated luminosity of 1 ab^{-1} . The shaded region of parameter space associated with each contour can be explored by the proposed collider at $\mathcal{S} \geq 3$. Thus, we get the kinematic reach on the cut-off scale Λ_{eff} at ILC for all relevant twist-2 lepto-philic and $U(1)_Y$ gauge Boson B-philic induced DM operators.

4.4 Differential Cross-sections and χ^2 Analysis

The photon transverse momentum ($p_{T\gamma}$) and photon pseudo-rapidity (η_γ) are found to be most sensitive kinematic observables for the process $e^+e^- \rightarrow \cancel{e} + \gamma$. To study the shape profile and its mass dependence we generate the normalized one dimensional distribution for the SM background processes and signals for the fermionic, real scalar and real vector DM candidates, keeping the respective effective coupling constant to be unity and rest to zero. We plot the normalized differential cross-sections for fixed Cut-Off scale $\Lambda_{\text{eff}} = 1$ TeV *w.r.t.* $p_{T\gamma}$ and η_γ induced by lepto-philic (i) Type-1 fermionic DM operators in figures 6a and 6e respectively, (ii) Type-2 fermionic DM operators in figures 6b and 6f respectively, (iii) Type-2 Scalar DM operators in figures 6c and 6g respectively, and (iv) Type-2 vector DM operators in figures 6d and 6h respectively. Each panel depict three shape profiles of the differential distribution corresponding to three choices of DM masses 75, 225 and 325 GeV respectively. Shaded rosy-brown and dark khaki histograms depict the normalized differential distributions *w.r.t.* $p_{T\gamma}$ in figures 6a, 6b, 6c, 6d and *w.r.t.* η_γ in figures 6e, 6f, 6g, 6h respectively for the background processes.

Repeating the same exercise for the B-philic operators, we depict the shape profile of the normalised differential distributions *w.r.t.* $p_{T\gamma}$ and η_γ corresponding to three choices of DM masses 75, 225 and 325 GeV induced by Type-1 fermionic, Type-2 fermionic, scalar and vector DM *w.r.t.* $p_{T\gamma}$ in figures 7a, 7b, 7c, 7d and *w.r.t.* η_γ in figures 7e, 7f, 7g, 7h respectively. The differential distributions for the background SM processes *w.r.t.* $p_{T\gamma}$ and η_γ are depicted in all of these figures and are shown in shaded rosy-brown and dark khaki histograms respectively.

We note that $p_{T\gamma}^{max}$ decreases with increase in DM mass. The shape of normalized distributions are comparatively more sensitive *w.r.t.* DM masses in case of the B-philic operators. This suggests that for the B-philic operators induced interactions, imposition of DM mass dependent dynamical cut can minimize the background and enhance the significance.

However, to enhance the sensitivity of the Λ_{eff} at a fixed coupling $\alpha_{T_i} = 1$ *w.r.t.* DM masses, we compute the χ^2 with the double differential distributions of kinematic observables $p_{T\gamma}$ and η_γ corresponding to the background and signal processes for (i) $50 \text{ GeV} \leq m_{\text{DM}} \leq 125 \text{ GeV}$ at $\sqrt{s} = 250 \text{ GeV}$ and an integrated luminosity of 250 fb^{-1} , (ii) $100 \text{ GeV} \leq m_{\text{DM}} \leq 250 \text{ GeV}$ at $\sqrt{s} = 500 \text{ GeV}$ and an integrated luminosity of 500 fb^{-1} , and (iii) $100 \text{ GeV} \leq m_{\text{DM}} \leq 500 \text{ GeV}$

at $\sqrt{s} = 1 \text{ TeV}$ and an integrated luminosity of 1 ab^{-1} . The χ^2 is defined as

$$\chi^2 \equiv \chi^2(m_{\text{DM}}, \alpha_{T_i}, \Lambda_{\text{eff}}) = \sum_{j=1}^{n_1} \sum_{i=1}^{n_2} \left[\frac{\frac{\Delta N_{ij}^{NP}}{(\Delta p_{T\gamma})_i (\Delta \eta_\gamma)_j}}{\sqrt{\frac{\Delta N_{ij}^{SM+NP}}{(\Delta p_{T\gamma})_i (\Delta \eta_\gamma)_j} + \delta_{\text{sys}}^2 \left\{ \frac{\Delta N_{ij}^{SM+NP}}{(\Delta p_{T\gamma})_i (\Delta \eta_\gamma)_j} \right\}^2}} \right]^2 \quad (22)$$

where ΔN_{ij}^{NP} and ΔN_{ij}^{SM+NP} are the number of differential New Physics and total events respectively in the two dimensional $[(\Delta p_{T\gamma})_i - (\Delta \eta_\gamma)_j]^{\text{th}}$ grid. Here δ_{sys} represents the total systematic error in the measurement.

We consider only one effective operator at time with the fixed coupling constant of unity and adopted a conservative value for the systematic error to be 1%. We simulate the two-dimension differential distributions using the collider parameters as given in Table 1 and choosing the basic selection cuts. In addition we impose DM mass dependent dynamical cuts to minimize the background for $U(1)_Y$ gauge Boson B-philic induced interactions, which translates into an acceptance dynamical cut on the photon energy

$$E_\gamma \leq \frac{s - 4m_{\text{DM}}^2}{2\sqrt{s}}. \quad (23)$$

We plot the 3σ contours at 99.73% C.L. in the $m_{\text{DM}} - \Lambda_{\text{eff}}$ for lepto-philic and B-philic operators in figures 8a and 8d respectively corresponding to $\sqrt{s} = 250 \text{ GeV}$ with an integrated luminosity of 250 fb^{-1} , figures 8b and 8e correspond to 3σ contours at 99.73% C.L. in the $m_{\text{DM}} - \Lambda_{\text{eff}}$ for lepto-philic and B-philic operators for $\sqrt{s} = 500 \text{ GeV}$ with an integrated luminosity of 500 fb^{-1} . We also give the 3σ contours at 99.73% C.L. for an upgraded high luminosity ILC operating at $\sqrt{s} = 1 \text{ TeV}$ with an integrated luminosity of 1 ab^{-1} in figures 8c and 8f corresponding to interactions induced by lepto-philic and B-philic operators respectively.

We observe that the kinematic reach of the Λ_{eff} is enhanced 5-6 times in comparison to that obtained from the naive significance analysis. The B-philic operators showed better response to the χ^2 analysis based on the double differential distributions which was expected from their one dimensional distribution shown in figure 7.

5 Summary and Outlook

The recent constraints derived from the observation on the dwarf spheroidal satellite galaxies in Fermi-LAT [24–26], excess in electron/positron channel around 10

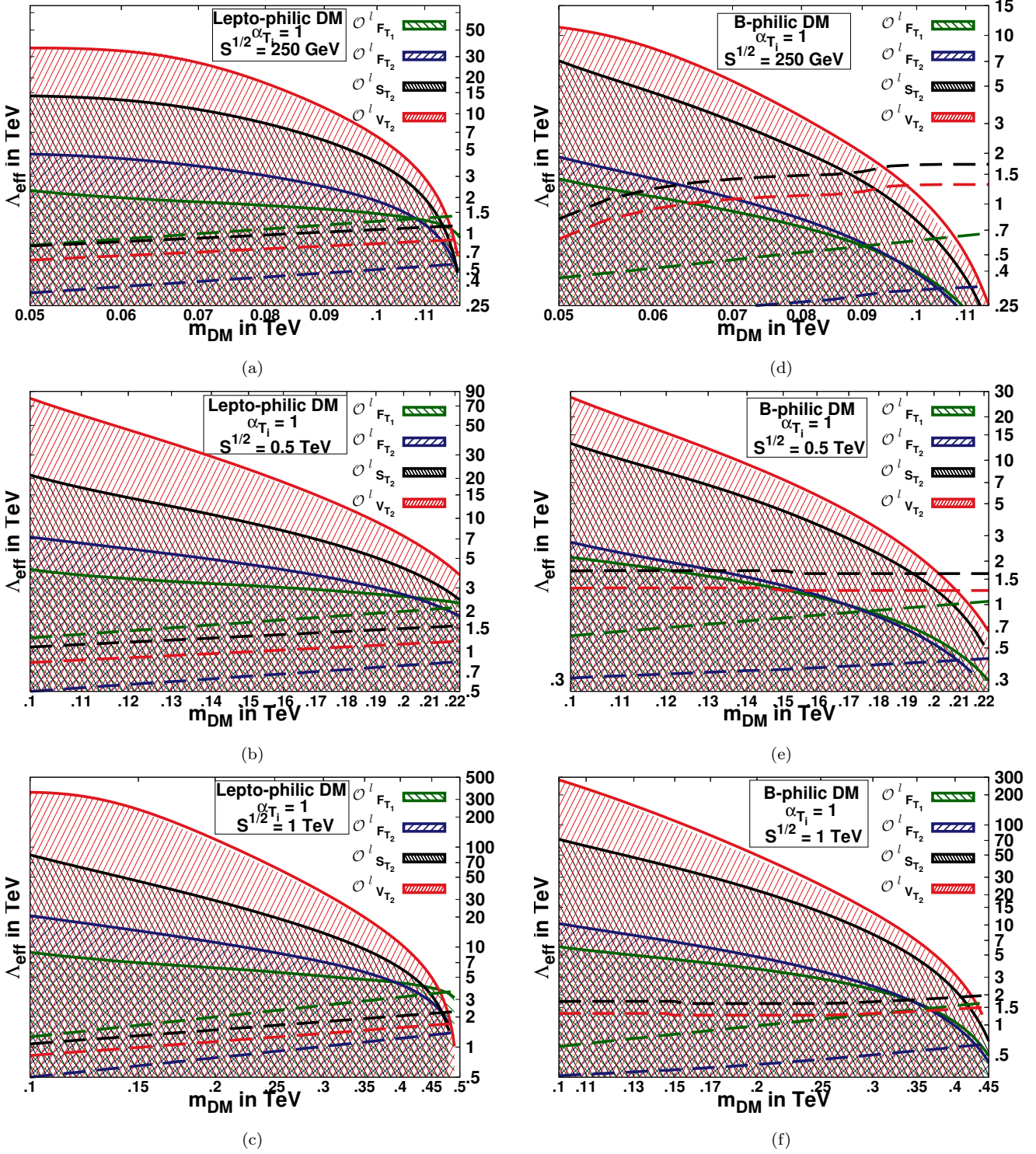


Fig. 8: Solid lines depict 3σ with 99.73 % C.L. contours in the $m_{\text{DM}} - \Lambda_{\text{eff}}$ plane from the χ^2 analyses of the $e^+e^- \rightarrow \cancel{E}_T + \gamma$ signature at the proposed ILC designed for (i) $\sqrt{s} = 250$ GeV with an integrated luminosity 250 fb^{-1} in figures 8a and 8d, (ii) $\sqrt{s} = 500$ GeV with an integrated luminosity 500 fb^{-1} in figures 8b and 8e, and (iii) $\sqrt{s} = 1$ TeV with an integrated luminosity 1 ab^{-1} in figures 8c and 8f respectively. Each figure contain four contours corresponding to the twist-2 Type-1 fermionic and Type-2 fermionic, scalar and vector operators respectively. The enclosed shaded region corresponding to the respective contour is accessible for discovery with $\geq 99.73\%$ C.L. The regions below the colored dashed lines corresponding to respective four operators satisfy the relic density constraint $\Omega_{\text{DM}} h^2 \leq 0.1199 \pm 0.0022$.

GeV at PAMELA [30,31], excess in flux of electrons/positrons around 400-500 GeV at ATIC [32] and PPB-BETS [33] balloon experiments and exclusion of quark channels by AMS-02 data [28, 29] hints toward the existence of non-baryonic DM. This implies that the direct detection experiments have to be sensitive on the recoil momentum of the atom or an electron in DM - atom and/or DM - electron scattering respectively due to suppressed loop-level interactions of DM with the quarks in the nucleon. Characterization for such lepto-philic and electro-weak gauge Boson B-philic DM particles are likely to be difficult and challenging at the LHC and therefore it becomes imperative to probe the sensitivity of the associated DM pair production channels at the proposed lepton collider ILC. Motivated by these observations and restrictions, we have explored the viable alternative stable non-baryonic spin 1/2, 0 and 1 DM particles $\sim 10 - 1000$ GeV, contributing to the relic density through their super-weak interactions with twist-2 leptonic and $U(1)_Y$ gauge Boson currents in a model independent approach. In this article, we have considered the super-symmetric and Extra-Dimensional models inspired effective second rank twist interactions of the leptons and gauge Bosons with the spin 1/2, 0 and 1 DM candidates.

We have listed a minimal set of the twist-2 operators corresponding to lepto-philic and $U(1)_Y$ gauge Boson tensor currents in section 2 which couples to the tensor currents generated by the bi-linears of the DM fields. These DM operators contribute

We have analytically calculated the thermalized annihilation cross-sections for the fermionic, scalar and vector DM induced by lepto-philic (A.10) - (A.13) and B-philic (A.14) - (A.17) operators respectively, which are in agreement numerically with that of MadDM. The relic density contours satisfying the PLANCK observations depict the upper bound on Λ_{eff} for fixed coupling $\alpha_{T_i} = 1$ in the $m_{\text{DM}} - \Lambda_{\text{eff}}$ as shown in figures 1a, 1b and 1c for the lepto-philic, τ^\pm -philic and B-philic DM interactions respectively. Using these upper bounds on Λ_{eff} for a given m_{DM} , we estimated the thermally averaged annihilation indirect detection cross-section for lepto-philic and τ^\pm -philic or electro-philic in figures 2a and 2b respectively are compared with that obtained from Fermi-LAT [24–26], while thermally averaged annihilation indirect detection cross-section for B-philic DM shown in figure 2c is compared with the observations from H.E.S.S. data [27]. We find that the present experimental limits in the respective searches not only favours the allowed parameter space from the relic density, but also constraints the DM model by providing the lower bound on the $\Lambda_{\text{eff, min}}$ for a given DM mass at fixed coupling α_{T_i} .

We have computed the elastic DM - free electron direct detection scattering cross-section analytically only for lepto-philic induced interactions and depicted in figure 3 as the τ^\pm -philic and B-philic DM interactions do not have any tree level interactions either with the atom or the nucleon. Although the contribution of the loops are suppressed but they need to be investigated for the complete study of the twist-2 operators. On superimposing inelastic DM - atom scattering cross-section from DAMA [77]. XENON100T [78] we observe that the parameter space allowed by the relic density is shrunk and we get a conservative lower limit on the cut-off at fixed coupling $\alpha_{T_i} = 1$ for a given DM mass. We have analysed the bound state effects of the electron and derived the analytical expressions for the event rate [77].

Next, we probed and compared the $3\text{-}\sigma$ efficiency of DM production processes $e^+e^- \rightarrow \cancel{E}_T + \gamma^* \rightarrow \cancel{E}_T + l^+l^-$ and $e^+e^- \rightarrow \cancel{E}_T + \gamma$ at ILC induced through twist-2 interactions of lepto-philic and B-philic interactions for $m_{\text{DM}} \sim 50 - 400$ GeV as shown in table 2. The 3σ significance contours for the dominant DM pair production in association with mono-photon at 99.73% C.L. are drawn *w.r.t.* SM background in figures 5a and 5d for lepto-philic and B-philic respectively at $\sqrt{s} = 250$ GeV and an integrated luminosity of 250 fb^{-1} , in figures 5b and 5e for lepto-philic and B-philic respectively at $\sqrt{s} = 500$ GeV and an integrated luminosity of 500 fb^{-1} and in figures 5c and 5f respectively for $\sqrt{s} = 1$ TeV and 1 ab^{-1} , with basic kinematic cuts in Table 1. We improve the sensitivity of the Λ_{eff} by minimizing the χ^2 using the optimal variable technique on the 2-D distributions *w.r.t.* $p_{T,\gamma}$ and η_γ for the three stages of the proposed collider (i) at $\sqrt{s} = 250$ GeV with an integrated luminosity of 250 fb^{-1} , (ii) at $\sqrt{s} = 500$ GeV with an integrated luminosity of 500 fb^{-1} and (iii) at $\sqrt{s} = 1$ TeV with an integrated luminosity of 1 ab^{-1} . The three sigma contours for χ^2 analysis in $m_{\text{DM}} - \Lambda_{\text{eff}}$ plane are drawn in figures 8a and 8d corresponding to the lepto-philic and B-philic respectively for case (i) and similarly, contours corresponding to case (ii) and case (iii) are shown in figures 8b, 8e and 8c, 8f respectively.

We hope this study will be useful in studying the physics potential of the ILC in context to dark matter searches.

Acknowledgements HB and SD thank Mihoko Nojiri and Mamta Dahiya for discussions and suggestions throughout the work. HB acknowledges the CSIR-JRF fellowship. HB and SD acknowledge the partial financial support from the CSIR grant No. 03(1340)/15/ EMR-II. SD thanks the Theory Division, KEK, for an excellent hospitality where this problem was conceived.

Appendix A: Thermal averaged annihilation cross-sections

The fermionic, scalar and vector DM pair annihilation cross sections to SM l^+l^- pairs of mass m_l induced by the *lepto-philic* twist-2 operators are given by

$$\sigma_{T_1}^{\text{ann}}(\chi\bar{\chi} \rightarrow l^+l^-) = \frac{\pi\alpha_{T_1}^2}{s} \left(\frac{m_\chi^2}{\Lambda_{\text{eff}}^6} \right) \sqrt{\frac{s-4m_l^2}{s-4m_\chi^2}} \times \left[16m_l^2 m_\chi^2 + 32m_\chi^4 + \left(9m_l^2 m_\chi^2 - \frac{11}{3}m_l^4 + \frac{14}{3}m_\chi^4 \right) |\mathbf{v}|^2 \right] \quad (\text{A.1})$$

$$\sigma_{T_2}^{\text{ann}}(\chi\bar{\chi} \rightarrow l^+l^-) = \frac{\pi\alpha_{T_2}^2}{s} \left(\frac{m_\chi^2}{\Lambda_{\text{eff}}^6} \right) \sqrt{\frac{s-4m_l^2}{s-4m_\chi^2}} m_l^2 (m_\chi^2 - m_l^2) |\mathbf{v}|^2 \quad (\text{A.2})$$

$$\sigma_S^{\text{ann}}(\phi^0\phi^0 \rightarrow l^+l^-) = \frac{\pi\alpha_{\phi^0}^2}{s} \left(\frac{m_{\phi^0}^2}{\Lambda_{\text{eff}}^4} \right) \sqrt{\frac{s-4m_l^2}{s-4m_{\phi^0}^2}} \times \left[2m_l^2 - \frac{2m_l^4}{m_{\phi^0}^2} + \left(\frac{4}{3}m_l^4 + \frac{11}{6}m_l^2 + \frac{16}{3}m_{\phi^0}^2 \right) |\mathbf{v}|^2 \right] \quad (\text{A.3})$$

$$\sigma_V^{\text{ann}}(V^0V^0 \rightarrow l^+l^-) = \frac{\pi\alpha_{V^0}^2}{s} \left(\frac{m_{V^0}^2}{\Lambda_{\text{eff}}^4} \right) \sqrt{\frac{s-4m_l^2}{s-4m_{V^0}^2}} \times \left[\frac{2}{3}m_l^2 - \frac{2}{3}\frac{m_l^4}{m_{V^0}^2} + \left(\frac{2}{9}\frac{m_l^4}{m_{V^0}^2} + \frac{5}{6}m_l^2 + \frac{16}{9}m_{V^0}^2 \right) |\mathbf{v}|^2 \right] \quad (\text{A.4})$$

The fermionic, scalar and vector DM pair annihilation cross sections to photon pairs induced by the $U(1)_Y$ *Boson B-philic* twist-2 operators are given by

$$\sigma_{T_1}^{\text{ann}}(\chi\bar{\chi} \rightarrow \gamma\gamma) = \frac{8\pi\alpha_{T_1}^2}{3s} \cos^2\theta_W \frac{m_\chi^6}{\Lambda_{\text{eff}}^6} \sqrt{\frac{s}{s-4m_\chi^2}} |\mathbf{v}|^2 \quad (\text{A.5})$$

$$\sigma_{T_2}^{\text{ann}}(\chi\bar{\chi} \rightarrow \gamma\gamma) = \frac{\pi\alpha_{T_2}^2}{s} \cos^2\theta_W \frac{m_\chi^6}{\Lambda_{\text{eff}}^6} \sqrt{\frac{s}{s-4m_\chi^2}} |\mathbf{v}|^2 \quad (\text{A.6})$$

$$\sigma_S^{\text{ann}}(\phi^0\phi^0 \rightarrow \gamma\gamma) = \frac{2\pi\alpha_{\phi^0}^2}{s} \cos^2\theta_W \frac{m_{\phi^0}^4}{\Lambda_{\text{eff}}^4} \sqrt{\frac{s}{s-4m_{\phi^0}^2}} \left[1 + \frac{2}{3} |\mathbf{v}|^2 \right] \quad (\text{A.7})$$

$$\sigma_V^{\text{ann}}(V^0V^0 \rightarrow \gamma\gamma) = \frac{2\pi\alpha_{V^0}^2}{3s} \cos^2\theta_W \frac{m_{V^0}^4}{\Lambda_{\text{eff}}^4} \sqrt{\frac{s}{s-4m_{V^0}^2}} [1 + |\mathbf{v}|^2] \quad (\text{A.8})$$

where θ_W is the Weinberg mixing angle.

The DM relic density is given in terms of thermally averaged DM annihilation cross sections $\langle\sigma_{\text{ann}}|\mathbf{v}|\rangle$ in equation (12). To compute the same we express the relative velocity of DM pair in the laboratory frame $|\mathbf{v}|$

in terms of c.m. energy \sqrt{s} as

$$|\mathbf{v}| = \frac{\sqrt{s(s-4m_{\text{DM}}^2)}}{s-2m_{\text{DM}}^2}. \quad (\text{A.9})$$

Since $v \ll c$, for non-relativistic DM we expand $s = 4m_{\text{DM}}^2 + m_{\text{DM}}^2 |\mathbf{v}|^2 + \frac{3}{4}m_{\text{DM}}^2 |\mathbf{v}|^4 + \mathcal{O}(|\mathbf{v}|^6)$ and compute the thermally averaged annihilation cross sections for lepto-philic and $U(1)_Y$ gauge Boson-philic DM respectively.

Thermal averaged annihilation cross-sections corresponding to the cross-sections given in equations (A.1) - (A.4) for the lepto-philic operators are given respectively as

$$\langle\sigma_{T_1}^{\text{ann}}|\mathbf{v}|\rangle(\chi\bar{\chi} \rightarrow l^+l^-) = \pi\alpha_{T_1}^2 \left(\frac{m_\chi^4}{\Lambda_{\text{eff}}^6} \right) \sqrt{1 - \frac{m_l^2}{m_\chi^2}} \times \left[1 + \frac{m_l^2}{2m_\chi^2} - \frac{34}{96} \frac{6}{x_F} \right] \quad (\text{A.10})$$

$$\langle\sigma_{T_2}^{\text{ann}}|\mathbf{v}|\rangle(\chi\bar{\chi} \rightarrow l^+l^-) = \frac{\pi\alpha_{T_2}^2}{2} \left(\frac{m_l^2 m_\chi^2}{\Lambda_{\text{eff}}^6} \right) \times \left[1 - \frac{m_l^2}{m_\chi^2} \right]^{\frac{3}{2}} \frac{6}{x_F} \quad (\text{A.11})$$

$$\langle\sigma_S^{\text{ann}}|\mathbf{v}|\rangle(\phi^0\phi^0 \rightarrow l^+l^-) = \pi\alpha_{\phi^0}^2 \left(\frac{m_{\phi^0}^2}{\Lambda_{\text{eff}}^4} \right) \sqrt{1 - \frac{m_l^2}{m_{\phi^0}^2}} \times \left[\frac{m_l^2}{m_{\phi^0}^2} - \frac{m_l^4}{m_{\phi^0}^4} + \left(\frac{8}{3} + \frac{11}{12} \frac{m_l^2}{m_{\phi^0}^2} + \frac{2}{3} \frac{m_l^4}{m_{\phi^0}^4} \right) \frac{6}{x_F} \right] \quad (\text{A.12})$$

$$\langle\sigma_V^{\text{ann}}|\mathbf{v}|\rangle(V^0V^0 \rightarrow l^+l^-) = \frac{8\pi\alpha_{V^0}^2}{9} \left(\frac{m_{V^0}^2}{\Lambda_{\text{eff}}^4} \right) \sqrt{1 - \frac{m_l^2}{m_{V^0}^2}} \times \left[\frac{3}{8} \frac{m_l^2}{m_{V^0}^2} - \frac{3}{8} \frac{m_l^4}{m_{V^0}^4} + \left(1 + \frac{15}{32} \frac{m_l^2}{m_{V^0}^2} + \frac{1}{8} \frac{m_l^4}{m_{V^0}^4} \right) \frac{6}{x_F} \right] \quad (\text{A.13})$$

Similarly, the annihilation cross-sections given in equations (A.5)-(A.8) for the $U(1)_Y$ gauge Boson B-philic operators are thermalized to give the following thermal averaged annihilation cross-sections:

$$\langle\sigma_{T_1}^{\text{ann}}|\mathbf{v}|\rangle(\chi\bar{\chi} \rightarrow \gamma\gamma) = \frac{4\pi\alpha_{T_1}^2}{3} \cos^2\theta_W \left(\frac{m_\chi^4}{\Lambda_{\text{eff}}^6} \right) \frac{6}{x_F} \quad (\text{A.14})$$

$$\langle\sigma_{T_2}^{\text{ann}}|\mathbf{v}|\rangle(\chi\bar{\chi} \rightarrow \gamma\gamma) = \frac{4\pi\alpha_{T_2}^2}{2} \cos^2\theta_W \left(\frac{m_\chi^4}{\Lambda_{\text{eff}}^6} \right) \frac{6}{x_F} \quad (\text{A.15})$$

$$\langle\sigma_S^{\text{ann}}|\mathbf{v}|\rangle(\phi^0\phi^0 \rightarrow \gamma\gamma) = \pi\alpha_{\phi^0}^2 \cos^2\theta_W \left(\frac{m_{\phi^0}^2}{\Lambda_{\text{eff}}^4} \right) \left[1 + \frac{1}{6} \frac{6}{x_F} \right] \quad (\text{A.16})$$

$$\langle\sigma_V^{\text{ann}}|\mathbf{v}|\rangle(V^0V^0 \rightarrow \gamma\gamma) = \frac{\pi\alpha_{V^0}^2}{3} \cos^2\theta_W \left(\frac{m_{V^0}^2}{\Lambda_{\text{eff}}^4} \right) \left[1 + \frac{1}{2} \frac{6}{x_F} \right] \quad (\text{A.17})$$

References

1. G. Bertone, D. Hooper and J. Silk, *Phys. Rept.* **405**, 279 (2005) doi:10.1016/j.physrep.2004.08.031 [hep-ph/0404175].
2. V. C. Rubin and W. K. Ford, Jr., *Astroph. J.* **159** (1970) 379.
3. L. A. Moustakas and R. B. Metcalf, *Mon. Not. Roy. Astron. Soc.* **339**, 607 (2003) doi:10.1046/j.1365-8711.2003.06055.x [astro-ph/0206176].
4. M. Milgrom, *Astrophys. J.* **270**, 365 (1983). doi:10.1086/161130
5. D. Clowe, M. Bradac, A. H. Gonzalez, M. Markevitch, S. W. Randall, C. Jones and D. Zaritsky, *Astrophys. J.* **648**, L109 (2006) doi:10.1086/508162 [astro-ph/0608407].
6. E. van Uitert *et al* *Astron. Astroph.* **545** A71(2012) [arXiv:1206.4304].
7. E. Komatsu *et al.* [WMAP Science Team], *PTEP* **2014**, 06B102 (2014) doi:10.1093/ptep/ptu083 [arXiv:1404.5415 [astro-ph.CO]].
8. P. A. R. Ade *et al.* [Planck Collaboration], *Astron. Astrophys.* **594**, A13 (2016) doi:10.1051/0004-6361/201525830 [arXiv:1502.01589 [astro-ph.CO]].
9. T. M. Hong, arXiv:1709.02304 [hep-ex].
10. F. Kahlhoefer, *Int. J. Mod. Phys. A* **32**, no. 13, 1730006 (2017) doi:10.1142/S0217751X1730006X [arXiv:1702.02430 [hep-ph]].
11. V. A Mitsou, **2015** *J. Phys.: Conf. Ser.* 651 012023 doi:10.1088/1742-6596/651/1/012023.
12. H. Dreiner, M. Huck, M. KrAdmer, D. Schmeier and J. Tattersall, *Phys. Rev. D* **87**, no. 7, 075015 (2013) doi:10.1103/PhysRevD.87.075015 [arXiv:1211.2254 [hep-ph]].
13. M. Battaglia and M. E. Peskin, *eConf C* **050318**, 0709 (2005) [hep-ph/0509135].
14. S. Dutta, D. Sachdeva and B. Rawat, *Eur. Phys. J. C* **77**, no. 9, 639 (2017) doi:10.1140/epjc/s10052-017-5188-8 [arXiv:1704.03994 [hep-ph]].
15. R. Bernabei *et al.*, *Eur. Phys. J. C* **73**, 2648 (2013) doi:10.1140/epjc/s10052-013-2648-7 [arXiv:1308.5109 [astro-ph.GA]].
16. R. Bernabei *et al.*, *Universe* **4** (2018) no.11, 116 [Nucl. Phys. Atom. Energy **19** (2018) no.4, 307] doi:10.3390/universe4110116, 10.15407/jnpae2018.04.307 [arXiv:1805.10486 [hep-ex]].
17. C. E. Aalseth *et al.* [CoGeNT Collaboration], *Phys. Rev. D* **88**, 012002 (2013) doi:10.1103/PhysRevD.88.012002 [arXiv:1208.5737 [astro-ph.CO]].
18. G. Angloher *et al.* [CRESST Collaboration], *Eur. Phys. J. C* **77**, no. 5, 299 (2017) doi:10.1140/epjc/s10052-017-4878-6 [arXiv:1612.07662 [hep-ex]].
19. R. Agnese *et al.* [CDMS Collaboration], *Phys. Rev. Lett.* **111** (2013) no.25, 251301 doi:10.1103/PhysRevLett.111.251301 [arXiv:1304.4279 [hep-ex]].
20. E. Aprile *et al.* [XENON100 Collaboration], *Phys. Rev. D* **94** (2016) no.12, 122001 doi:10.1103/PhysRevD.94.122001 [arXiv:1609.06154 [astro-ph.CO]].
21. E. Aprile *et al.* [XENON Collaboration], *Eur. Phys. J. C* **77** (2017) no.12, 881 doi:10.1140/epjc/s10052-017-5326-3 [arXiv:1708.07051 [astro-ph.IM]].
22. D. S. Akerib *et al.* [LUX Collaboration], *Phys. Rev. Lett.* **118** (2017) no.2, 021303 doi:10.1103/PhysRevLett.118.021303 [arXiv:1608.07648 [astro-ph.CO]].
23. X. Cui *et al.* [PandaX-II Collaboration], *Phys. Rev. Lett.* **119** (2017) no.18, 181302 doi:10.1103/PhysRevLett.119.181302 [arXiv:1708.06917 [astro-ph.CO]].
24. M. Ackermann *et al.* [Fermi-LAT Collaboration], *Phys. Rev. Lett.* **115** (2015) no.23, 231301 doi:10.1103/PhysRevLett.115.231301 [arXiv:1503.02641 [astro-ph.HE]].
25. M. Ajello *et al.* [Fermi-LAT Collaboration], *Astrophys. J.* **819** (2016) no.1, 44 doi:10.3847/0004-637X/819/1/44 [arXiv:1511.02938 [astro-ph.HE]].
26. A. Albert *et al.* [Fermi-LAT and DES Collaborations], *Astrophys. J.* **834** (2017) no.2, 110 doi:10.3847/1538-4357/834/2/110 [arXiv:1611.03184 [astro-ph.HE]].
27. A. Abramowski *et al.* [H.E.S.S. Collaboration], *Phys. Rev. Lett.* **110** (2013) 041301 doi:10.1103/PhysRevLett.110.041301 [arXiv:1301.1173 [astro-ph.HE]].
28. M. Aguilar *et al.* [AMS Collaboration], *Phys. Rev. Lett.* **113** (2014) 121102. doi:10.1103/PhysRevLett.113.121102
29. M. Aguilar *et al.* [AMS Collaboration], *Phys. Rev. Lett.* **117** (2016) no.9, 091103. doi:10.1103/PhysRevLett.117.091103
30. O. Adriani *et al.* [PAMELA Collaboration], *Phys. Rev. Lett.* **111**, 081102 (2013) doi:10.1103/PhysRevLett.111.081102 [arXiv:1308.0133 [astro-ph.HE]].
31. O. Adriani *et al.* [PAMELA Collaboration], *Nature* **458**, 607 (2009) doi:10.1038/nature07942 [arXiv:0810.4995 [astro-ph]].
32. A. D. Panov *et al.*, *Bull. Russ. Acad. Sci. Phys.* **71** (2007) 494 doi:10.3103/S1062873807040168 [astro-ph/0612377].
33. K. Yoshida, *et al.*, 42 (Nov., 2008) 1670-1675, doi:10.1016/j.asr.2007.04.043.
34. G. Ambrosi *et al.* [DAMPE Collaboration], *Nature* **552** (2017) 63 doi:10.1038/nature24475 [arXiv:1711.10981 [astro-ph.HE]].
35. T. Appelquist, H. C. Cheng and B. A. Dobrescu, *Phys. Rev. D* **64** (2001) 035002 doi:10.1103/PhysRevD.64.035002 [hep-ph/0012100].
36. J. Wess and B. Zumino, *Nucl. Phys. B* **70** (1974) 39. doi:10.1016/0550-3213(74)90355-1
37. H. P. Nilles, *Phys. Rept.* **110** (1984) 1. doi:10.1016/0370-1573(84)90008-5
38. M. Drees, R. Godbole, P. Roy, "Theory and phenomenology of sparticles: an account of four-dimensional N=1 supersymmetry in high energy physics" (2004).
39. N. Arkani-Hamed, A. G. Cohen, H. Georgy, *Phys. Lett. B* **513**,232-C240 (2001).
40. H. C. Cheng, I. Low, *JHEP* **0309**, 051 (2003), doi:10.1088/1126-6708/2003/09/051, [arXiv:hep-ph/0308199].
41. S. Dutta, A. Goyal and M. P. Singh, arXiv:1809.07877 [hep-ph].
42. J. M. Zheng, Z. H. Yu, J. W. Shao, X. J. Bi, Z. Li and H. H. Zhang, *Nucl. Phys. B* **854** (2012) 350 doi:10.1016/j.nuclphysb.2011.09.009 [arXiv:1012.2022 [hep-ph]].
43. A. Freitas and S. Westhoff, *JHEP* **1410** (2014) 116 doi:10.1007/JHEP10(2014)116 [arXiv:1408.1959 [hep-ph]].
44. K. G. Savvidy and J. D. Vergados, *Phys. Rev. D* **87** (2013) no.7, 075013 doi:10.1103/PhysRevD.87.075013 [arXiv:1211.3214 [hep-ph]].
45. C. F. Chang, X. G. He and J. Tandean, *Phys. Rev. D* **96** (2017) no.7, 075026 doi:10.1103/PhysRevD.96.075026 [arXiv:1704.01904 [hep-ph]].
46. S. Dutta, A. Goyal and L. K. Saini, *JHEP* **1802** (2018) 023 doi:10.1007/JHEP02(2018)023 [arXiv:1709.00720 [hep-ph]].
47. M. O. Khojali, A. Goyal, M. Kumar and A. S. Cornell, *Eur. Phys. J. C* **78** (2018) no.11, 920 doi:10.1140/epjc/s10052-018-6407-7 [arXiv:1705.05149 [hep-ph]].
48. M. O. Khojali, A. Goyal, M. Kumar and A. S. Cornell, *Eur. Phys. J. C* **77** (2017) no.1, 25 doi:10.1140/epjc/s10052-016-4589-4 [arXiv:1608.08958 [hep-ph]].

49. A. Boveia and C. Doglioni, *Ann. Rev. Nucl. Part. Sci.* **68**, 429 (2018) doi:10.1146/annurev-nucl-101917-021008 [arXiv:1810.12238 [hep-ex]].
50. S. Chatrchyan *et al.* [CMS Collaboration], *JHEP* **1212**, 034 (2012) doi:10.1007/JHEP12(2012)034 [arXiv:1210.3844 [hep-ex]].
51. G. Aad *et al.* [ATLAS Collaboration], *Phys. Rev. Lett.* **112**, no. 23, 231806 (2014) doi:10.1103/PhysRevLett.112.231806 [arXiv:1403.5657 [hep-ex]].
52. N. F. Bell, Y. Cai, R. K. Leane and A. D. Medina, *Phys. Rev. D* **90**, no. 3, 035027 (2014) doi:10.1103/PhysRevD.90.035027 [arXiv:1407.3001 [hep-ph]].
53. B. Bhattacharjee, D. Choudhury, K. Harigaya, S. Matsumoto and M. M. Nojiri, *JHEP* **1304** (2013) 031 doi:10.1007/JHEP04(2013)031 [arXiv:1212.5013 [hep-ph]].
54. R. C. Cotta, J. L. Hewett, M. P. Le and T. G. Rizzo, *Phys. Rev. D* **88** (2013) 116009 doi:10.1103/PhysRevD.88.116009 [arXiv:1210.0525 [hep-ph]].
55. J. Y. Chen, E. W. Kolb and L. T. Wang, *Phys. Dark Univ.* **2** (2013) 200 doi:10.1016/j.dark.2013.11.002 [arXiv:1305.0021 [hep-ph]].
56. A. Crivellin, U. Haisch and A. Hibbs, *Phys. Rev. D* **91** (2015) 074028 doi:10.1103/PhysRevD.91.074028 [arXiv:1501.00907 [hep-ph]].
57. N. Chen, J. Wang and X. P. Wang, arXiv:1501.04486 [hep-ph].
58. P. J. Fox, R. Harnik, J. Kopp and Y. Tsai, *Phys. Rev. D* **85** (2012) 056011 doi:10.1103/PhysRevD.85.056011 [arXiv:1109.4398 [hep-ph]].
59. Y. J. Chae and M. Perelstein, “*Dark Matter Search at a Linear Collider: Effective Operator Approach*”, *JHEP* **1305** (2013) 138 [arXiv:1211.4008 [hep-ph]].
60. N. F. Bell, J. B. Dent, A. J. Galea, T. D. Jacques, L. M. Krauss and T. J. Weiler, *Phys. Rev. D* **86** (2012) 096011 doi:10.1103/PhysRevD.86.096011 [arXiv:1209.0231 [hep-ph]].
61. D. J. Gross and F. Wilczek, *Phys. Rev. D* **9**, 980 (1974). doi:10.1103/PhysRevD.9.980
62. M. Drees and M. Nojiri, *Phys. Rev. D* **48** (1993) 3483 doi:10.1103/PhysRevD.48.3483 [hep-ph/9307208].
63. J. Hisano, K. Ishiwata and N. Nagata, *Phys. Rev. D* **82** (2010) 115007 doi:10.1103/PhysRevD.82.115007 [arXiv:1007.2601 [hep-ph]].
64. J. Hisano, K. Ishiwata, N. Nagata and M. Yamanaka, *Prog. Theor. Phys.* **126** (2011) 435 doi:10.1143/PTP.126.435 [arXiv:1012.5455 [hep-ph]].
65. J. Hisano, K. Ishiwata, N. Nagata and T. Takesako, *JHEP* **1107** (2011) 005 doi:10.1007/JHEP07(2011)005 [arXiv:1104.0228 [hep-ph]].
66. J. Hisano, K. Ishiwata and N. Nagata, *Phys. Lett. B* **706** (2011) 208 doi:10.1016/j.physletb.2011.11.017 [arXiv:1110.3719 [hep-ph]].
67. J. Hisano, K. Ishiwata and N. Nagata, *Phys. Rev. D* **87** (2013) 035020 doi:10.1103/PhysRevD.87.035020 [arXiv:1210.5985 [hep-ph]].
68. J. Hisano, R. Nagai and N. Nagata, *JHEP* **1505** (2015) 037 doi:10.1007/JHEP05(2015)037 [arXiv:1502.02244 [hep-ph]].
69. J. Hisano, K. Ishiwata and N. Nagata, *JHEP* **1506** (2015) 097 doi:10.1007/JHEP06(2015)097 [arXiv:1504.00915 [hep-ph]].
70. A. Ibarra and S. Wild, *JCAP* **1505** (2015) no.05, 047 doi:10.1088/1475-7516/2015/05/047 [arXiv:1503.03382 [hep-ph]].
71. J. Herrero-Garcia, E. Molinaro and M. A. Schmidt, *Eur. Phys. J. C* **78** (2018) no.6, 471 doi:10.1140/epjc/s10052-018-5935-5 [arXiv:1803.05660 [hep-ph]].
72. J. Hisano, R. Nagai and N. Nagata, *JHEP* **1812** (2018) 059 doi:10.1007/JHEP12(2018)059 [arXiv:1808.06301 [hep-ph]].
73. J. Kumar and D. Marfatia, *Phys. Rev. D* **88** (2013) no.1, 014035 doi:10.1103/PhysRevD.88.014035 [arXiv:1305.1611 [hep-ph]].
74. F. Ambrogio, C. Arina, M. Backovic, J. Heisig, F. Maltoni, L. Mantani, O. Mattelaer and G. Mohlabeng, arXiv:1804.00044 [hep-ph].
75. J. Alwall *et al.*, *JHEP* **1407** (2014) 079 doi:10.1007/JHEP07(2014)079 [arXiv:1405.0301 [hep-ph]].
76. A. Alloul, N. D. Christensen, C. Degrande, C. Duhr and B. Fuks, *Comput. Phys. Commun.* **185** (2014) 2250 doi:10.1016/j.cpc.2014.04.012 [arXiv:1310.1921 [hep-ph]].
77. J. Kopp, V. Niro, T. Schwetz and J. Zupan, “*DAMA/LIBRA and leptonically interacting Dark Matter*”, *Phys. Rev. D* **80**, 083502 (2009) [arXiv:0907.3159 [hep-ph]].
78. E. Aprile *et al.* [XENON100 Collaboration], “*Exclusion of Leptophilic Dark Matter Models using XENON100 Electronic Recoil Data*”, *Science* **349**, no. 6250, 851 (2015) doi:10.1126/science.aab2069 [arXiv:1507.07747 [astro-ph.CO]].
79. S. Schael *et al.* [ALEPH and DELPHI and L3 and OPAL and LEP Electroweak Collaborations], *Phys. Rept.* **532**, 119 (2013) doi:10.1016/j.physrep.2013.07.004 [arXiv:1302.3415 [hep-ex]].
80. M. Aaboud *et al.* [ATLAS Collaboration], *Eur. Phys. J. C* **77** (2017) no.6, 393 doi:10.1140/epjc/s10052-017-4965-8 [arXiv:1704.03848 [hep-ex]].
81. T. Behnke *et al.*, arXiv:1306.6329 [physics.ins-det].
82. T. Behnke *et al.*, “*The International Linear Collider Technical Design Report - Volume 1: Executive Summary*,” arXiv:1306.6327 [physics.acc-ph].
83. E. Conte and B. Fuks, *Int. J. Mod. Phys. A* **33**, no. 28, 1830027 (2018) doi:10.1142/S0217751X18300272 [arXiv:1808.00480 [hep-ph]].
84. E. Conte, B. Fuks and G. Serret, *Comput. Phys. Commun.* **184**, 222 (2013) doi:10.1016/j.cpc.2012.09.009 [arXiv:1206.1599 [hep-ph]].